**TECHNISCHE
UNIVERSITÄT
WIEN**

DIPLOMA THESIS

LSNA Characterization and Calibration

supervised by

Ass. Prof. Dipl.-Ing. Dr.techn. Holger Arthaber
and
Univ.Ass. Dipl.-Ing. Dr.techn. Thomas Faseth

performed at the
Institute of Electrodymamics, Microwave and Circuit Engineering

by

Daniel Amberger, BSc.
Matr.Nr. 1228511
Kirchstraße 16, D-94234 Viechtach

Vienna, March 2016

Abstract

Vector network analyzers (VNA) and scattering parameter measurements are commonly used to characterize devices and components in the small-signal regime. While VNA measurements allow a full characterization of linear elements, they fail for non-linear elements, like for power amplifiers or other active circuits driven at high power levels. To get a better insight in a device's nonlinear properties, VNA-measurements are typically extended by spectrum analyzer, time-domain, or load-pull (LP) measurements. But even the combination of all these measurements has limitations. Here, the so-called large signal network analyzer (LSNA) provides a solution: It allows capturing a device's nonlinear effects based on a traceable nonlinear calibration standard.

Recently, the documentation of the Sampling Downconverter Agilent N4464A, which is an integral part of the commercial LSNA system available at the Institute of Electrodynamics, Microwave and Circuit Engineering, became public domain. Because the existing system and software framework experiences some limitations, e.g. for broadband signal characterization, a modified and extended LSNA platform has been developed.

First, the realized LSNA system updated the previous non-flexible software implementation by a fully custom implementation of the LSNA software and calibration framework using Matlab. Second, different broadband calibration and measurement techniques for arbitrary periodic signals utilizing arbitrary measurement frequency grids have been introduced and verified in this thesis. The realized Matlab LSNA software framework assists the user in the stages of instrument initialization, calibration, and the measurement itself. The setup verification measurements demonstrate proper operation of the LSNA system and high accuracy of the calibration for the targeted applications.

The flexibility of the LSNA was increased enormously compared to the commercial system. For example, applications like broadband load-pull waveform engineering under pulsed periodic excitation are now possible.

Kurzfassung

Messungen der Streuparameter mit vektoriellen Netzwerkanalysatoren
(VNA) werden häufig eingesetzt, um das Kleinsignalverhalten von
Bauelementen zu beschreiben. Während mit VNA Messungen die
vollständige Beschreibung von linearen Bauteilen möglich ist, ver-
sagen diese bei nichtlinearen Elementen. Um besseren Einblick in
die nichtlinearen Eigenschaften eines Bauteils zu erhalten, werden ty-
pischerweise Messungen im Zeitbereich, Spektrumanalysatoren, oder
„load pull"-Systeme eingesetzt, deren Möglichkeiten aber sogar durch
Kombination aller Methoden begrenzt ist. Der sogenannte „large sig-
nal netwok analyzer" (LSNA) bietet eine Lösung: Basierend auf einem
rückführbaren Kalibrationsnormal können nichtlineare Effekte erfasst
werden.

Vor kurzem wurde die Dokumentation des Agilent N4464A „Samp-
ling Downconverter" öffentlich verfügbar, der ein Hauptbestandteil
des kommerziell erhältlichen LSNA-Systems ist und dem Institute of
Electrodynamics, Microwave and Circuit Engineering zur Verfügung
steht. Da das bestehende System und dessen Software Einschränkun-
gen im Bezug auf breitbandige Messungen besitzt, wurde im Ver-
lauf dieser Diplomarbeit eine erweiterte LSNA-Plattform entwickelt.
Dafür wurden verschiedene breitbandige Kalibrierungs- und Messver-
fahren für periodische Signale mit beliebigen Messfrequenzrastern ent-
wickelt und verifiziert. Das realisierte LSNA-System ersetzt die wenig
flexible vorhandene Software durch ein in Matlab implementiertes
Software-Framework. Die geschaffene LSNA-Software unterstützt den
Benutzer bei der Initialisierung der Geräte, der Kalibrierung und bei
der Messung selbst.

Verifikationsmessungen bestätigten die korrekte Funktion des Systems
und zeigten eine hohe Genauigkeit für die angestrebten Anwendungs-
gebiete. Die Flexibilität des entstandenen LSNAs konnte im Vergleich
zum kommerziellen System enorm gesteigert werden. Anwendungen,
wie z.B. Breitband „load pull" im Zusammenhang mit sogenanntem
„waveform engineering" sind nun möglich.

Hiermit erkläre ich, dass die vorliegende Arbeit gemäß dem Code of Conduct - Regeln zur Sicherung guter wissenschaftlicher Praxis (in der aktuellen Fassung des jeweiligen Mitteilungsblattes der TU Wien), insbesondere ohne unzulässige Hilfe Dritter und ohne Benutzung anderer als der angegebenen Hilfsmittel, angefertigt wurde. Die aus anderen Quellen direkt oder indirekt übernommenen Daten und Konzepte sind unter Angabe der Quelle gekennzeichnet. Die Arbeit wurde bisher weder im In- noch im Ausland in gleicher oder in ähnlicher Form in anderen Prüfungsverfahren vorgelegt.

Wien, 1. April 2016

Contents

Abbreviations

AC	...	alternating current
ADC	...	analog to digital converter
CF	...	crest factor
CIS	...	coherent interleaved sampling mode
CW	...	continuous wave
DC	...	direct current
DAC	...	digital to analog converter
DFT	...	discrete Fourier transform
DUT	...	device under test
EMCE	...	Institute of Electrodynamics, Microwave and Circuit Engineering
GPIB	...	general purpose interface bus
GUI	...	graphical user interface
HP	...	Hewlett Packard
HPR	...	harmonic phase reference
IF	...	intermediate frequency
IQ	...	inphase/quadrature
LAN	...	local area network
LO	...	local oscillator
LRM	...	load reflect match
LSNA	...	large signal network analyzer
LTI	...	linear time invariant
MMIC	...	monolithic microwave integrated circuit
NMDG	...	Network Measurement and Description Group
NNMS	...	non-linear network measurement system
NVNA	...	non-linear vector network analyzer
MTA	...	microwave transition analyzer
PLL	...	phase locked loop
PWM	...	pulse width modulation
RF	...	radio frequency
SCPI	...	standardized commands for programmable instruments
SFDR	...	spurious free dynamic range
SNR	...	signal to noise ratio
SOLT	...	short open load thru
SRD	...	step recovery diode
TRL	...	thru reflect load
VNA	...	vector network analyzer
VUB	...	Frije Universiteit Brussel

Chapter 1

Introduction

A classical vector network analyzer (VNA) is suitable to fully characterize linear devices like filters or cables. In small-signal operation, even non-linear systems such as a transistor can be modelled as quasi-linear. For many years this approach has satisfied the needs for modelling non-linear components. Nowadays, the ongoing trend in communications applications is towards higher power drive levels. Devices are gradually pushed towards or beyond their boundary of small-signal operation. Thus, describing the system using linear models often becomes inappropriate and using linear models fails. Obviously, measuring S-parameters to characterize such components or systems, is no longer sufficient [1].

Widely used instruments such as spectrum analyzers, oscilloscopes, or load-pull measurement systems only consider certain aspects of the non-linear behavior [2]. On contrary, the large signal network analyzer (LSNA) provides a fully calibrated characterization under large-signal non-linear conditions. LSNA measurement results enable the users to study non-linear device behavior, to verify their designs, and to improve device models at the circuit level [2].

1.1 Motivation

The first implementation of the LSNA was a so-called sampler based instrument and was developed by Hewlett Packard (HP) in the early 90s [3]. With the introduction of the microwave transition analyzer (MTA) it was possible to directly measure phase and amplitude of fundamental and harmonic spectral components [4]. In 1993, a cooperation of researchers of the Vrije Universiteit Brussel (VUB) and the Network Measurement and Description Group (NMDG) developed the first prototype of today's LSNA.This instrument has been given different names over time [1]:

- non-linear vector network analyzer (NVNA)

- non-linear network measurement system (NNMS)

- large signal network analyzer (LSNA)

The commercially available LSNA system only supports a specific measurement setup and has a few limitations. For example, spectral components of the signals (carriers and harmonics) must be above 600 MHz. This is related to the minimum fundamental frequency of the utilized standard harmonic phase reference (HPR) generator, which is needed for calibration as discussed later in chapter 3. Also the modulated measurement bandwidth is limited to twice the intermediate frequency (IF) bandwidth [2]. But, in many cases, the required measurement frequency grid, is much lower than 600 MHz and the trend in modern communications applications is toward broadband modulation schemes.

Recently, the documentation of the Sampling Down Converter became public domain which will be discussed in chapter 4. Furthermore, in the last years also new phase references with a minimum fundamental frequency of 10 MHz are quite common. Because the existing software implementation of the LSNA hardware available at the Institute of Electrodynamics, Microwave and Circuit Engineering (EMCE) is quite non-flexible and outdated, the idea of this thesis was born to overcome some limitations by a custom LSNA software and calibration implementation. Thus, this diploma thesis provides techniques for calibrated measurements of arbitrary periodic signals using arbitrary frequency grids. The flexibility of the LSNA thereby can be increased enormously.

1.2   Application Examples

Practical examples for LSNA systems are covering a wide range of applications, like transistor characterization, load-pull waveform engineering, frequency-domain black-box modelling, state-space black-box modelling techniques, active digital-signal integrity measurements, and spectral regrowth measurements [3]. The LSNA is a powerful tool that offers many different representations of the acquired data.
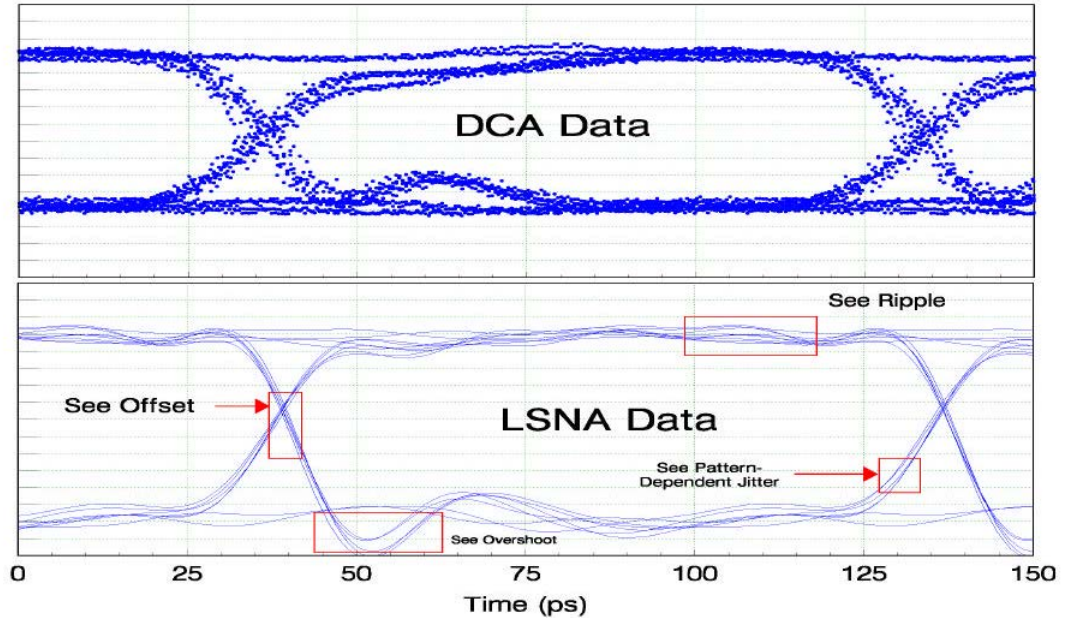
Figure 1.1: Measuring digital signals [3]

A further important application is the on-wafer measurement of high-speed digital signals as depicted in figure 1.1. The upper part contains a waveform obtained by the classic technique for performing such a measurement, a sampling oscilloscope. The probes, connectors, cables, and the instrument itself introduce significant distortions in the measurement of the eye-diagram. The synchronization of several channels of the scope is difficult, the noise performance is comparably worse, and the trajectories of the symbols cannot unambiguously be observed.

Performing similar measurements using an LSNA system results in fully error-corrected waveforms all the way up to the tip of the probe. In the lower part in figure 1.1 it is clear that the LSNA measurement has a better dynamic range than the oscilloscope measurement. Phenomena like ripple or overshoot can be detected. All the distortions are also present at the LSNA frequency down-converter. However, they can be compensated using an appropriate calibration procedure [3].

Chapter 2

Large Signal Network Analysis

Small signal analysis is based on signal levels that are small enough so that the devices operate in their linear region. However, many applications like power amplifiers drive the devices into their non-linear region of operation and thus the superposition principle is no longer valid. Device characterization using S-parameters is not sufficient and it is necessary to "go beyond S-parameters" [5]. The idea of large signal network analysis is to operate a device under test (DUT) under realistic large signal operating conditions and to completely and accurately acquire the information of its electrical behavior. This allows the designer to gain a deep understanding of the device. It can be accomplished by measuring the voltage and current time domain waveforms at both input and output. For example, the acquired data can be used to construct a behavioral model [6]. The purpose of the LSNA was to build an absolute wave meter that captures the whole spectrum in a single take [1]. Absolute magnitudes and phase relationships between all measurement frequencies of the forward and backward travelling waves a and b at the ports of a device (shown in figure 2.1) under large signal operation are measured.
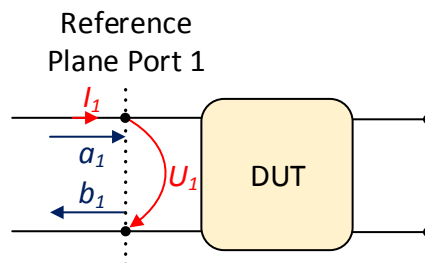
Figure 2.1: Normalized waves at a two-port DUT

In many cases it is advantageous to analyze the voltage and current wave-forms. Due to the definition of travelling waves, given by equation 2.1, also for LSNA measurements the user can switch between a, b and voltage U and current representation I. Z_0 equals the characteristic impedance which is 50 Ω in most cases. The relations are given by

$$a = \frac{U + Z_0 \cdot I}{2\sqrt{Z_0}}, \quad b = \frac{U - Z_0 \cdot I}{2\sqrt{Z_0}} \qquad (2.1)$$

and

$$U = \sqrt{Z_0}(a + b), \quad I = \frac{a - b}{\sqrt{Z_0}} \qquad (2.2)$$

Moreover, because of the available phase relationships between all measurement frequencies, it is possible to choose between time and frequency domain.

2.1   Sampler Based Principle

The four channel sampling downconverter can be considered as the core of the large signal network analyzer. A schematic of the downconverter is depicted in figure 2.2. Microwave signals up to many GHz can be downconverted and compressed to an intermediate frequency (IF) spectrum.

The local oscillator (LO) source contains a fractional-N synthesizer which is programmable between 10 and 25 MHz with a resolution of 1 Hz. It is phase locked to a stable 10 MHz reference signal. The stability and precision of the reference source significantly influences the overall system performance. A step recovery diode (SRD) forms sampling pulses at the frequency of the LO source which are split on the four mixers. This pulses are then multiplied with the RF signal by a harmonic mixer, as described in more detail in section 2.1.1. At the output of the harmonic sampler many harmonic mixing products are present. If the LO frequency is properly chosen every frequency component of the radio frequency (RF) signal is unambiguously contained within the IF bandwidth at least once. This corresponds to a low frequency compression of the RF signal.
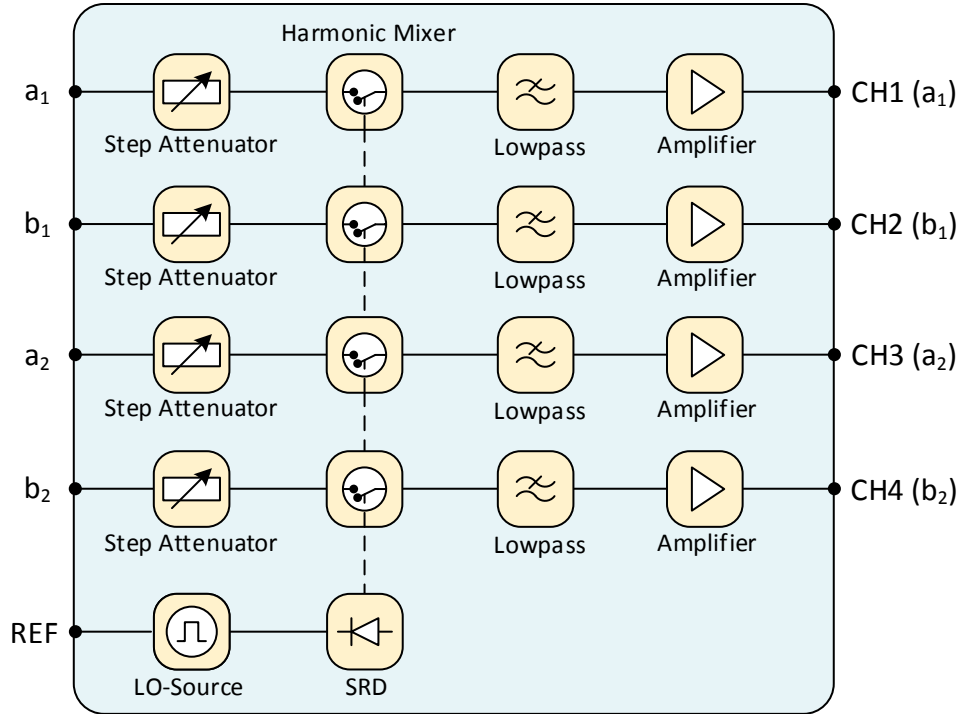
Figure 2.2: Simplified schematic of a four channel sampling downconverter

A detailed mathematical description of the harmonic sampling theory is also given in section 2.1.1. For the approach of harmonic sampling, the RF signal and LO frequency must satisfy certain requirements which are described in more detail in section 2.1.2.

2.1.1 Harmonic Sampling Theory
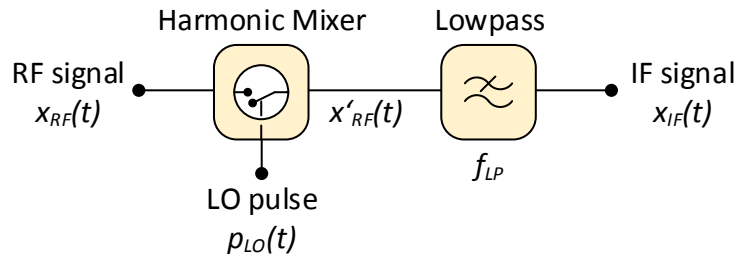
Figure 2.3: Harmonic sampling principle

The basic idea of harmonic sampling idea is depicted in figure 2.3. For the

sake of simplicity only one harmonic signal $x_{RF}(t)$ is considered at the RF input. Its complex amplitude is $A = A_{RF}e^{-j\phi_{RF}}$ while the frequency is denoted by f_{RF}.

$$
\begin{aligned}
x_{RF}(t) &= A_{RF}\cos(2\pi f_{RF}t - \phi_{RF}) \\
&= \frac{1}{2}\left[A_{RF}e^{j(2\pi f_{RF}t-\phi_{RF})} + A_{RF}e^{-j(2\pi f_{RF}t-\phi_{RF})}\right] \\
&= \frac{1}{2}\left[Ae^{j(2\pi f_{RF}t)} + A^{*}e^{-j(2\pi f_{RF}t)}\right]
\end{aligned}
\tag{2.3}
$$

Due to the linearity principle, more complex input signals can be composed using the superposition principle. The sampling pulse train is considered to be ideal and is formed by an infinite number of delayed Dirac delta functions

$$
p_{LO}(t) = \sum_{n=-\infty}^{\infty} \delta\left(t - \frac{n}{f_{LO}}\right)
\tag{2.4}
$$

The harmonic mixing process corresponds to a multiplication of the input signal $x_{RF}(t)$ and the pulse train $p_{LO}(t)$. At the mixer output, the signal $x'_{RF}(t)$ is given by

$$
\begin{aligned}
x'_{RF}(t) &= x_{RF}(t) \cdot p_{LO}(t) \\
&= \frac{1}{2}\left[Ae^{j(2\pi f_{RF}t)} + A^{*}e^{-j(2\pi f_{RF}t)}\right] \cdot \sum_{n=-\infty}^{\infty} \delta\left(t - \frac{n}{f_{LO}}\right)
\end{aligned}
\tag{2.5}
$$

Because of the properties of the Fourier transform a multiplication in time domain will become a convolution in frequency domain, denoted by "$*$". Fourier transformation of $x'_{RF}(t)$ results in

$$
\begin{aligned}
X'_{RF}(f) &= \left(X_{RF} * P_{LO}\right)(f) \\
&= \frac{1}{2}\left[A\delta(f - f_{RF}) + A^{*}\delta(f + f_{RF})\right] * \sum_{n=-\infty}^{\infty} \delta(f - nf_{LO}) \\
&= \frac{A}{2}\sum_{n=-\infty}^{\infty} \delta[f - (f_{RF} - nf_{LO})] + \frac{A^{*}}{2}\sum_{m=-\infty}^{\infty} \delta[f - (mf_{LO} - f_{RF})]
\end{aligned}
\tag{2.6}
$$

where signals in frequency domain representation are denoted by upper-case letters. It can be seen that the input signal appears at the output of the harmonic mixer as a series of convolutional products. They are located in regular shape at frequencies of $f_{RF} - nf_{LO}$ and in inverted shape at $mf_{LO} - f_{RF}$. The

mixing products are equally spaced at a distance of f_{LO}. The output signal of the harmonic mixer is lowpass filtered before being processed further (see figure 2.3. Assuming an ideal lowpass with a cut-off frequency of f_{LP} leads to an IF output signal with a frequency f_{IF} and a complex amplitude A_{IF} of

$$f_{IF} = \begin{cases} f_{RF} \bmod f_{LO}, & \text{if } f_{RF} \bmod f_{LO} < f_{LP} \\ (-f_{RF} \bmod f_{LO}), & \text{if } (-f_{RF} \bmod f_{LO}) < f_{LP} \\ 0, & \text{else} \end{cases}$$

and

$$A_{IF} = \begin{cases} \frac{1}{2}A, & \text{if } f_{RF} \bmod f_{LO} < f_{LP} \\ \frac{1}{2}A^{*}, & \text{if } (-f_{RF} \bmod f_{LO}) < f_{LP} \\ 0, & \text{else} \end{cases} \tag{2.7}$$

which can be found in a similar manner in [7]. It can be seen from equation 2.7 that a deterministic relationship exists between frequencies and phases, respectively a linear relationship between the amplitudes, at the RF input and the IF output of the downconverter. This relationship even holds true for non-ideal pulses and a non-ideal lowpass filter, up to certain limits which will be discussed in more detail in section 3.1.
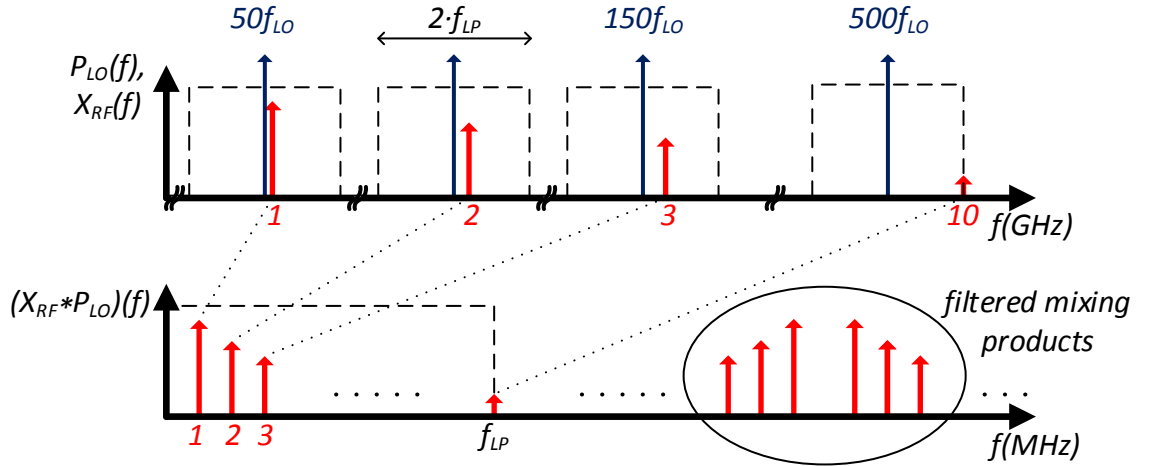
Figure 2.4: Illustration of the downconversion process

A practical example of the theory above is given in figure 2.4. The signal at the RF input has a 1 GHz fundamental together with 9 harmonics. The LO signal of 19.98 MHz is used to shift the signal to the IF located at 1 MHz $(= 1\,\text{GHz} - 50\,f_{LO})$. Accordingly, the 10th harmonic at 10 GHz is converted to

10 MHz in the IF. Consequently, the result at the IF output is a frequency compressed version of the RF signal. Finally, the IF signal is digitized utilizing a suitable ADC sampling frequency and number of samples. The spectral components are then obtained by applying a discrete Fourier transform (DFT). Based on the same principle, harmonic sampling even works for more complex (narrow- or broadband modulated) signals. However, according to the described principle the input signals must have a discrete frequency spectrum, which refers to periodic input signals. It should be noted that the IF signal is not a low frequency copy of the RF signal in general. The downconverted frequency components in the IF signal are usually scrambled in a more complex, but unique manner.

2.1.2   Practical Limitations

In order to perform accurate LSNA measurements, several requirements must be satisfied. The most important are

> ***Periodic Signals – Time-invariant Systems***
> Due to harmonic sampling, as described in section 2.1.1, the RF signals must be periodic. The periodicity at both DUT ports must be the same and constant over time [4]. Systems which show a time-variant behavior can not be characterized.

> ***Maximum RF Frequency***
> As shown in figure 2.5, the sampling pulses are not ideal (as considered in equation 2.4) The finite fall time, which is much shorter than the rise time, causes a conversion loss towards higher frequencies. For a typical fall time of 10 ps, the loss due to conversion is about 3 dB at 44 GHz [8]. Between the RF input connector and the harmonic mixer additional transmission losses will be added. Because of these phenomena, it is necessary to define a maximum RF frequency.
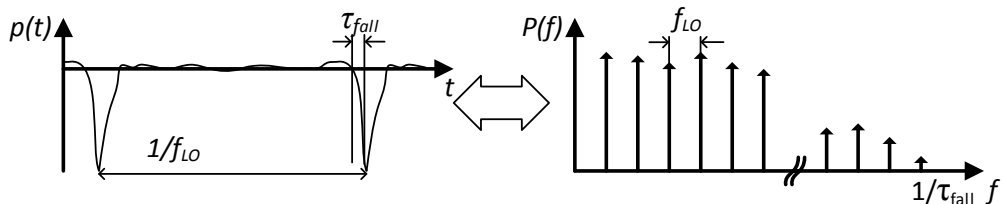
Figure 2.5: Realistic sampling pulse in time and frequency domain

Overlapping
For an increasing number of spectral tones, the signal is compressed into the IF bandwidth more and more. The local oscillator frequency must be selected in such way that the tones do not overlay in the frequency domain. Moreover, the tone spacing Δf should be as high as possible, as described in more detail in section 4.2.3. The theoretical limit is determined by $\Delta f_{max} = f_{LP}/N_{tones}$, where f_{LP} corresponds to the IF bandwidth and the number of tones at the RF input is denoted by N_{tones}.

RF/IF Harmonic Spacing
In practice the LO source is not perfectly stable. Phase noise at the output of the SRD causes a broadening of the sampling pulses in frequency domain, investigated in more detail in section 4.2.3. This relates to a minimum tone spacing at the RF input as well at the IF output. Consequently, the maximum number of tones is determined by the minimum tone spacing Δf_{min}: $N_{max} = f_{LP}/\Delta f_{min}$.
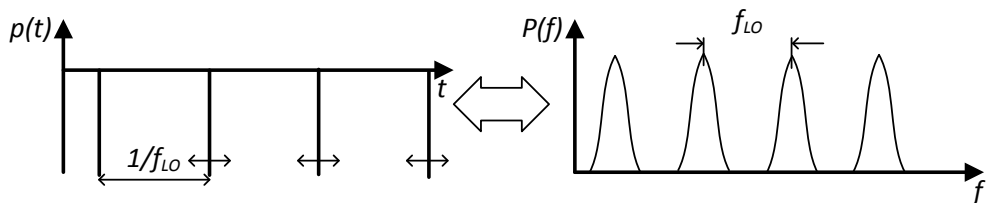
Figure 2.6: Sampling pulse which is affected with phase noise in time and frequency domain

2.1.3   RF-IF Mapping Technique

As mentioned above, more complex RF input signals which means signals that have a tone spacing much smaller than the LO frequency, usually result in IF signals that contain scrambled frequency components. Figure 2.7 shows a simple RF to IF frequency mapping utilizing 25 input frequencies that are equally spaced beginning at 20 MHz up to 500 MHz.
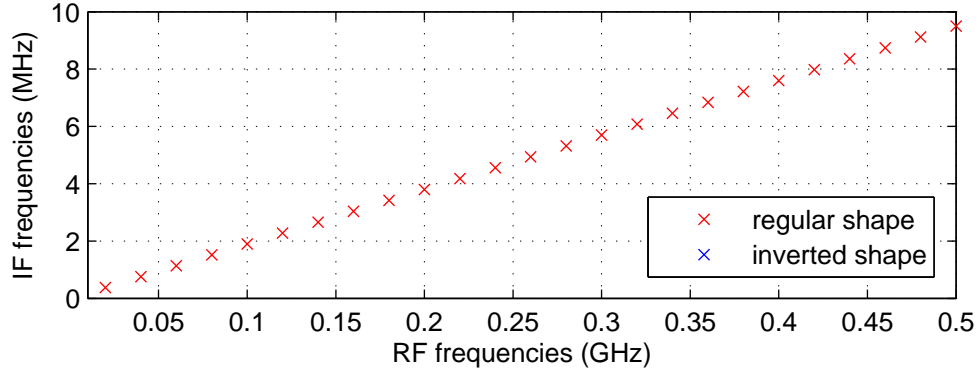
Figure 2.7: RF - IF frequency mapping. 20 MHz RF tone spacing

The tones are mixed down by an LO of 19.62 MHz according to equation 2.7. This will lead to an IF signal which also has equally spaced tones distributed over the entire IF bandwidth and its frequency indices n are equal to the frequency indices of the RF signal. This is due to the fact that the nth RF tone mixes down with the mth LO harmonic and m is an increasing function of n.
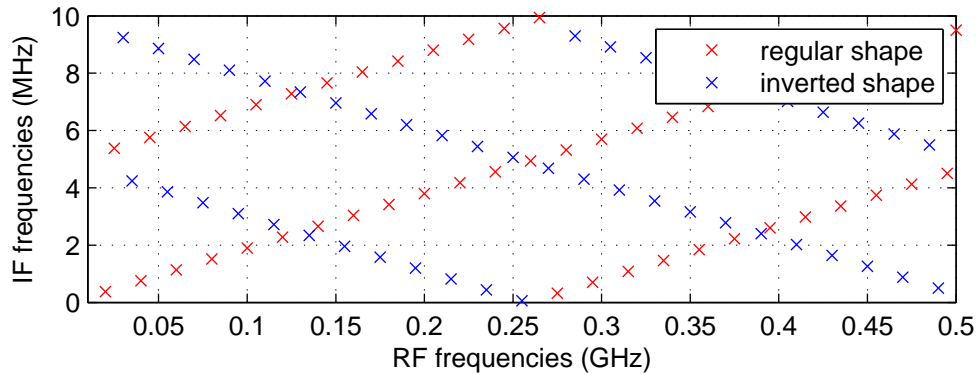
Figure 2.8: RF - IF frequency mapping. 5 MHz RF tone spacing

The RF path configuration of the instrument remained the same for figure 2.8, but compared to figure 2.7 a frequency spacing of the input tones of 5 MHz was set up. In this case, the IF signal contains scrambled frequency components in regular and in inverted shape. However, if multiple RF tones do not coincide at the same IF position a unique mapping exists. Consequently, each IF tone can be returned to its correct RF frequency position. Frequency components appearing in inverted shape must be additionally conjugated. This process is called "descrambling".

2.2 LSNA Hardware Overview

An LSNA consists of several modules as depicted in the general schematic of a two-port system in figure 2.9. The DUT can be excited at one or both ports by an RF source. This can be a microwave source or a vector signal generator. The spectral components of the incident and scattered waves a_1^D, b_1^D, a_2^D, b_2^D at the ports of the DUT are separated and individually sensed by a test set as a_1^M, b_1^M, a_2^M, b_2^M. In the simplest case it can consist of four couplers. The sensed signals are attenuated to a certain level before they are sent to the sampling downconverter. This is done to handle a broad range of input powers, while keeping the sampling converter hardware itself within its linear region of operation. The downconverter operates according to the harmonic sampling principle, as described in section 2.1 and is in fact the key component of the system (depicted in detail in figure 2.2).
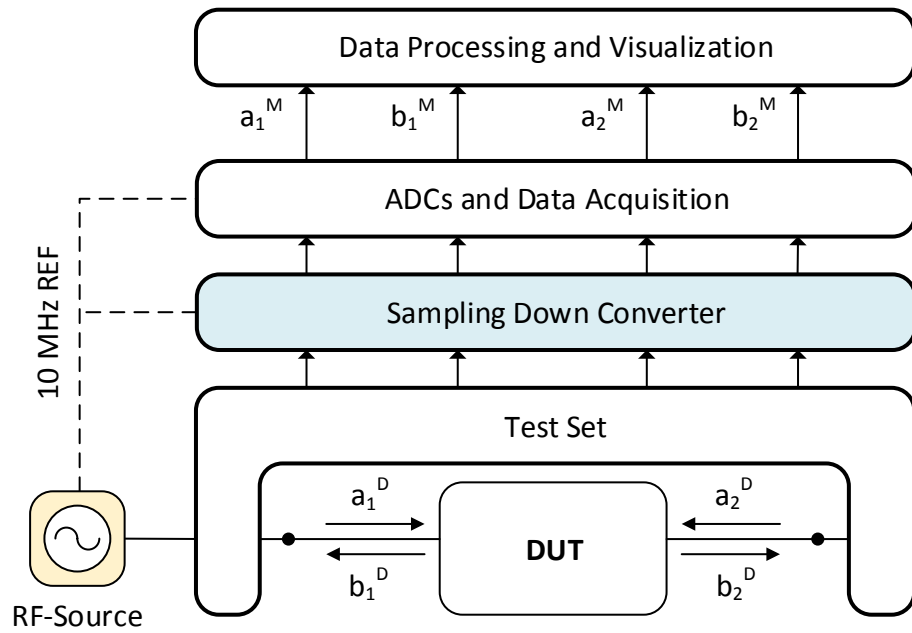
Figure 2.9: Main building blocks of generic two port LSNA

The resulting IF signals are amplified before being digitized by four synchronized analog to digital converters (ADCs). The downconverter, RF source, and ADCs are provided with the same reference clock to obtain a fully synchronized phase coherent measurement system. Finally, the data processing, visualization, and storage is done by a PC system.

In contrast to a VNA, the source is not a part of the measurement system, what enables a very flexible system. Furthermore, additional synthesizers for signal generation, amplifiers, tuners, or other components can be added.

Chapter 3

Calibration Theory

All hardware components of the measurement system introduce considerable distortions. In order to perform accurate and high resolution measurements, the systematic errors have to be eliminated. This can be done by an appropriate calibration procedure. The calibration must be performed for each measurement frequency [9] and consists of three main steps:

- a classical relative calibration

- a power calibration

- and a phase calibration

These steps are described in detail in the following sections. All models, procedures, and calculations in this chapter refer to connectorized devices. Nevertheless, the presented theory can be extended without any limitations to onwafer measurements [10].

3.1   Calibration Procedure Basics - Error Model

In an LSNA measurement, one wants to know the phases and amplitudes of a discrete set of spectral components at the DUT ports [3]. These incident and reflected waves are denoted by $a_1^D(f_n)$, $b_1^D(f_n)$, $a_2^D(f_n)$, $b_2^D(f_n)$. Starting from these values, further signal processing can be done. However, as shown in figure 2.9, there is only access to the distorted raw measured values $a_1^M(f_n)$, $b_1^M(f_n)$, $a_2^M(f_n)$, $b_2^M(f_n)$. Subscript 1 and 2 represent the device port number, while n denotes the frequency index.

The main requirement for calibrating the system is that the LSNA itself operates linearly and the settings are not changed. To avoid non-linear distortions, programmable step attenuators are used at the downconverter input (shown in figure 2.2). In the case of changing the attenuators, the calibration can be recalculated using section 3.6. If this assumption is valid, a linear relationship between the raw measured spectral components and the components at the DUT ports exists [8]. Because of the physical construction of the system, shown in figure 3.1, it is assumed that port 1 is fully isolated from port 2. Cross-coupling is only present due to the finite directivity of the couplers between channels 1 and 2, as well as between channels 3 and 4. Generally, such a model can be described as follows:

$$
\begin{pmatrix} a_1^D(f_n) \\ b_1^D(f_n) \\ a_2^D(f_n) \\ b_2^D(f_n) \end{pmatrix} = \begin{pmatrix} K(f_n) & \beta_1'(f_n) & 0 & 0 \\ \gamma_1'(f_n) & \delta_1'(f_n) & 0 & 0 \\ 0 & 0 & \alpha_2'(f_n) & \beta_2'(f_n) \\ 0 & 0 & \gamma_2'(f_n) & \delta_2'(f_n) \end{pmatrix} \begin{pmatrix} a_1^M(f_n) \\ b_1^M(f_n) \\ a_2^M(f_n) \\ b_2^M(f_n) \end{pmatrix}
\tag{3.1}
$$

Due to the linearity and the isolation assumption, an incident or reflected DUT frequency component is linearly associated to the measured values of the same port by a complex factor. In what follows, the frequency dependence (f_n) of a parameter is expressed by $a(f_n) = a_n$ for reasons of simplicity. Factoring out the complex $K_n = |K_n| e^{j\phi_K,n}$ leads to

$$
\begin{pmatrix} a_{1,n}^D \\ b_{1,n}^D \\ a_{2,n}^D \\ b_{2,n}^D \end{pmatrix} = K_n \begin{pmatrix} 1 & \beta_{1,n} & 0 & 0 \\ \gamma_{1,n} & \delta_{1,n} & 0 & 0 \\ 0 & 0 & \alpha_{2,n} & \beta_{2,n} \\ 0 & 0 & \gamma_{2,n} & \delta_{2,n} \end{pmatrix} \begin{pmatrix} a_{1,n}^M \\ b_{1,n}^M \\ a_{2,n}^M \\ b_{2,n}^M \end{pmatrix}
\tag{3.2}
$$

which can also be found in the literature in this form [8]. It contains the so-called "relative error coefficients" $\left\{ \alpha_{1,n}, \beta_{1/2,n}, \gamma_{1/2,n}, \delta_{1/2,n} \right\}$. Their determination is achieved by relative measurements, consequently referred to as relative calibration. K_n is denoted as the "absolute error coefficient", determined by an absolute power and an absolute phase calibration.
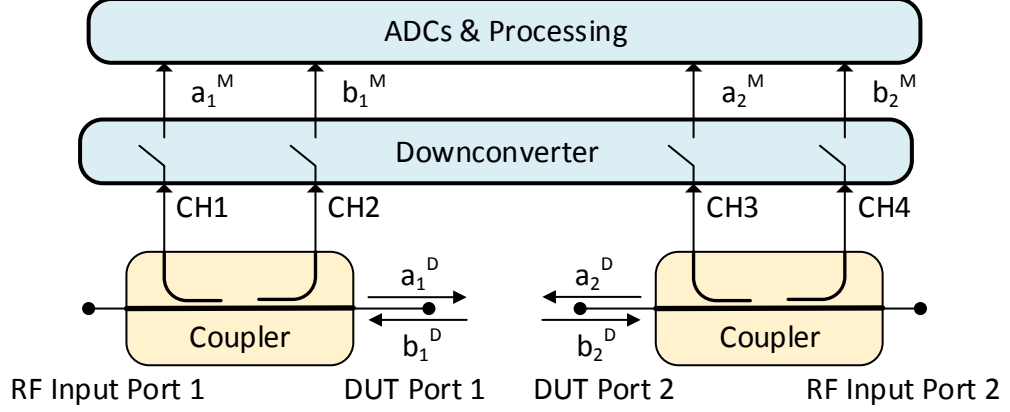
Figure 3.1: Simplified system model with all channel and port designations

From the above statements it follows that, the error model described in equation 3.2 can be separated into two linear equations:

$$\begin{pmatrix} a_{1,n}^D \\ b_{1,n}^D \end{pmatrix} = K_n \boldsymbol{T_{1,n}} \begin{pmatrix} a_{1,n}^M \\ b_{1,n}^M \end{pmatrix} \text{ and } \begin{pmatrix} a_{2,n}^D \\ b_{2,n}^D \end{pmatrix} = K_n \boldsymbol{T_{2,n}} \begin{pmatrix} a_{2,n}^M \\ b_{2,n}^M \end{pmatrix} \tag{3.3}$$

$\boldsymbol{T_{1,n}}$ and $\boldsymbol{T_{2,n}}$ are 2×2 matrices containing the relative error coefficients for each measurement frequency. The goal of the calibration process is to determine the relative and the absolute error coefficients. If these coefficients are known, the physical DUT quantities can be obtained by using equation 3.2 together with the raw measured quantities.

It should be noted that calibration would be possible even if cross-coupling between port 1 and 2 is present, but it would result in a more complex calibration.

3.2 Relative Calibration

The relative calibration is identical to the classical VNA calibration and can be established by the well known "short, open, load, thru" (SOLT), "thru, reflect, load" (TRL), "load, reflect, match" (LRM), or other calibrations [1]. Because an SOLT calibration has been implemented in this work, this method will be presented in the following.
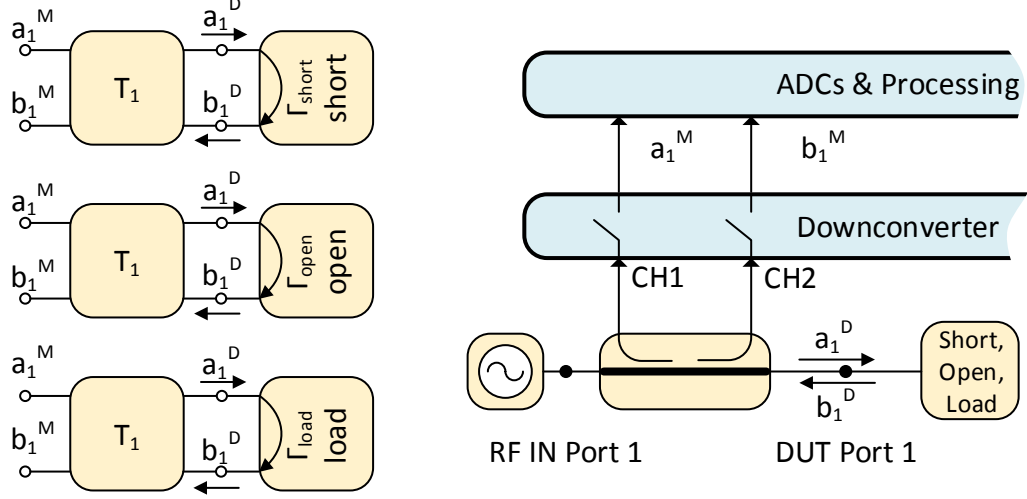
Figure 3.2: Relative calibration at port 1

To determine the seven relative error coefficients, at least seven raw measurements must performed for each frequency. The first three measurements are conducted using port 1 as RF source port at the DUT port 1. As depicted in figure 3.2 a short, an open, and a load is connected to the reference plane at port 1. As a consequence of nonideal calibration standards the reflection coefficients $\Gamma_{n,short}$, $\Gamma_{n,open}$, $\Gamma_{n,load}$ must been known for each frequency. The first three measurements result in ratios of:

$$\Gamma_{n,short} = \left(\frac{b_{1,n}}{a_{1,n}}\right)^{D}_{short} = \left(\frac{\gamma_{1,n}a^{M}_{1,n} + \delta_{1,n}b^{M}_{1,n}}{a^{M}_{1,n} + \beta_{1,n}b^{M}_{1,n}}\right)_{short}$$

$$\Gamma_{n,open} = \left(\frac{b_{1,n}}{a_{1,n}}\right)^{D}_{open} = \left(\frac{\gamma_{1,n}a^{M}_{1,n} + \delta_{1,n}b^{M}_{1,n}}{a^{M}_{1,n} + \beta_{1,n}b^{M}_{1,n}}\right)_{open}$$

$$\Gamma_{n,load} = \left(\frac{b_{1,n}}{a_{1,n}}\right)^{D}_{load} = \left(\frac{\gamma_{1,n}a^{M}_{1,n} + \delta_{1,n}b^{M}_{1,n}}{a^{M}_{1,n} + \beta_{1,n}b^{M}_{1,n}}\right)_{load} \tag{3.4}$$

where the unknown incident and reflected DUT waves have been substituted by the corresponding raw measured values using equation 3.2. Note that the absolute coefficient K_n can be cancelled out for ratios of the DUT values. This set of linear independent equations can easily be solved for the unknowns $\beta_{1,n}$,

$\gamma_{1,n}$, $\delta_{1,n}$ for each frequency using

$$
\begin{pmatrix} \beta_{1,n} \\ \gamma_{1,n} \\ \delta_{1,n} \end{pmatrix} = \begin{pmatrix} 1 & \left(\frac{b_{1,n}}{a_{1,n}}\right)^M_{short} & -\Gamma_{n,short}\left(\frac{b_{1,n}}{a_{1,n}}\right)^M_{short} \\ 1 & \left(\frac{b_{1,n}}{a_{1,n}}\right)^M_{open} & -\Gamma_{n,open}\left(\frac{b_{1,n}}{a_{1,n}}\right)^M_{open} \\ 1 & \left(\frac{b_{1,n}}{a_{1,n}}\right)^M_{load} & -\Gamma_{n,load}\left(\frac{b_{1,n}}{a_{1,n}}\right)^M_{load} \end{pmatrix}^{-1} \begin{pmatrix} \Gamma_{n,short} \\ \Gamma_{n,open} \\ \Gamma_{n,load} \end{pmatrix} \qquad (3.5)
$$
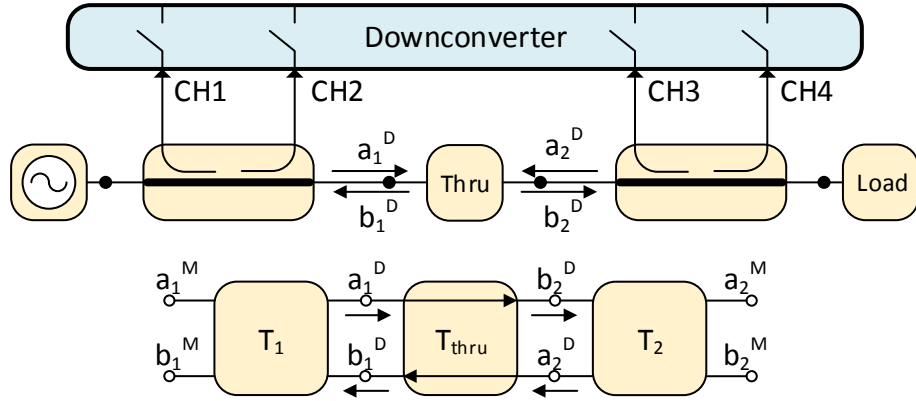
Figure 3.3: Thru calibration measurement

The second three calibration measurements have to be done in the same way as the first three measurements but are performed at DUT port 2. To determine the four unknowns in $\boldsymbol{T_{2,n}}$, an additional seventh measurement, as shown in figure 3.3, is required. Using a thru connection with a transmission factor $T_{n,thru}$, that is made between the DUT reference planes at port 1 and port 2, the following equation is obtained:

$$
T_{n,thru} = \left(\frac{b_{2,n}}{a_{1,n}}\right)^D_{thru} = \left(\frac{\gamma_{2,n}a_{2,n}^M + \delta_{2,n}b_{2,n}^M}{a_{1,n}^M + \beta_{1,n}b_{1,n}^M}\right)_{thru} \qquad (3.6)
$$

The fourth to the seventh measurement results in a set of four linear equations, that can be solved by

$$
\begin{pmatrix} \alpha_{2,n} \\ \beta_{2,n} \\ \gamma_{2,n} \\ \delta_{2,n} \end{pmatrix} = \begin{pmatrix} 1 & \left(\frac{b_{2,n}}{a_{2,n}}\right)^M_{short} & \Gamma_{n,short} & \Gamma_{n,short}\left(\frac{b_{2,n}}{a_{2,n}}\right)^M_{short} \\ 1 & \left(\frac{b_{2,n}}{a_{2,n}}\right)^M_{open} & \Gamma_{n,open} & \Gamma_{n,open}\left(\frac{b_{2,n}}{a_{2,n}}\right)^M_{open} \\ 1 & \left(\frac{b_{2,n}}{a_{2,n}}\right)^M_{load} & \Gamma_{n,load} & \Gamma_{n,load}\left(\frac{b_{2,n}}{a_{2,n}}\right)^M_{load} \\ 1 & \left(\frac{b_{2,n}}{a_{2,n}}\right)^M_{thru} & 0 & 0 \end{pmatrix}^{-1} \begin{pmatrix} 0 \\ 0 \\ 0 \\ \tilde{T}_{n,thru} \end{pmatrix} \qquad (3.7)
$$

with

$$\tilde{T}_{n,thru} = \left[\left(\frac{a_{1,n}}{a_{2,n}} \right)^M_{thru} + \left(\frac{b_{1,n}}{a_{2,n}} \right)^M_{thru} \beta_{1,n} \right] \cdot T_{n,thru} \tag{3.8}$$

When the relative calibration is finished, every matrix element of $\boldsymbol{T_{1,n}}$ and $\boldsymbol{T_{2,n}}$ is clearly defined. At this point, the LSNA could be used as a VNA to measure S parameters. For example, the calculation of the S_{11} parameter only requires the knowledge of the ratio

$$S_{11} = \frac{b^D_{1,n}}{a^D_{1,n}} = \frac{\gamma_{1,n}a^M_{1,n} + \delta_{1,n}b^M_{1,n}}{a^M_{1,n} + \beta_{1,n}b^M_{1,n}} \tag{3.9}$$

because only the relative error coefficients and the raw measurement quantities of a device have to be known when the source impedance is not changed between calibration and measurement.

3.3 Absolute Power Calibration

Starting from section 3.2, the remaining unknowns in the error model is the factor K_n. The following procedure describes how to determine its absolute value $|K_n|$ (again for each measurement frequency).
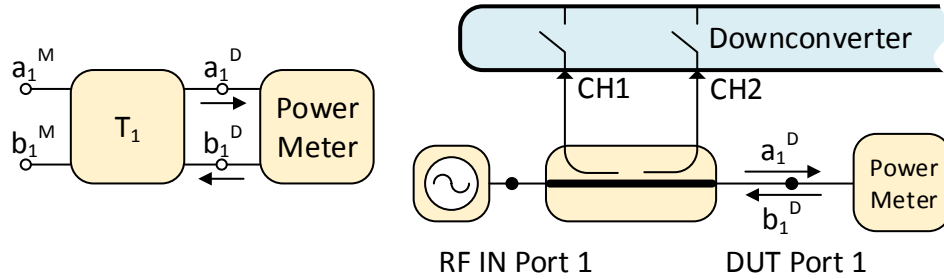
Figure 3.4: Power calibration

Because of well established, and precise power meters, it is common practice to perform this measurement by measuring the power at one DUT reference plane [10]. As shown in figure 3.4, a power sensor is connected to port 1. The incident wave $a_{1,n}$ into the power sensor is described by [11]

$$a^D_{1,n} = K_n \left(a^M_{1,n} + \beta_{1,n}b^M_{1,n} \right) \tag{3.10}$$

Consequently, a calibrated power meter measures the absolute power P_n [11], that can expressed by

$$P_n = \frac{\left|a_{1,n}^D\right|^2}{2} = \frac{\left|K_n\left(a_{1,n}^M + \beta_{1,n}b_{1,n}^M\right)\right|^2}{2}$$
$$= \frac{|K_n|^2}{2}\left|a_{1,n}^M + \beta_{1,n}b_{1,n}^M\right|^2 \tag{3.11}$$

The amplitude correction factor $|K_n|$ can be calculated using following equation:

$$|K_n| = \sqrt{\frac{2P_n}{\left|a_{1,n}^M + \beta_{1,n}b_{1,n}^M\right|}} \tag{3.12}$$

3.4 Phase Calibration

Determination of the one remaining unknown $\phi_{K,n} = \arg\left(K_n\right)$ is realized through the measurement of a known phase reference standard. It is connected directly to port 1, while the port 1 RF input is terminated, as at the right side in figure 3.5.
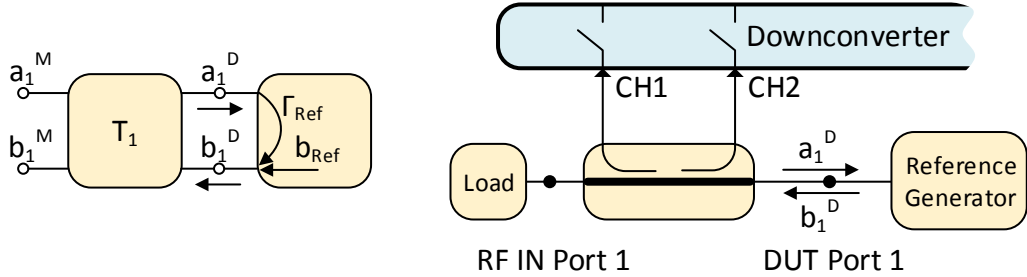
Figure 3.5: Phase calibration

The main difference to the previous calibrations is that a reference generator generates many (or all) spectral components at once and the phase relationships between all the tones are assumed stable and known with sufficient accuracy. Measuring the phase relationship with the LSNA and comparing it with the known phase relationship of the reference, allows to determine the phase factor $\phi_{K,n}$ [12]. Two different types of of calibrated generators are used to realize the phase calibration. The first is a comb generator, which is generally referred as harmonic phase reference (HPR). This strategy is discussed in section 3.4.1. The second approach, described in section 3.4.2, is based on a arbitrary waveform generator that is used as a microwave multisine source.

3.4.1   HPR Phase Calibration

A harmonic phase reference is a pulse generator that generates a large number of harmonic frequencies $n\omega_0$ with a stable and per-characterized phase relationship [3]. Typically, it consists of a step recovery diode and a pulse shaping non-linear transmission line. Alternatively, such as in the U9391F Agilent module shown in figure 3.6, a monolithic microwave integrated circuit (MMIC) is used to generate the pulses [10].

Figure 3.6: Agilent U9391F comb generator ($10\,\mathrm{MHz}$ to $50\,\mathrm{GHz}$)

The advantage is that frequency components of the pulses cover a wide bandwidth up to many GHz. However, each frequency component only contains a low amount of energy because of the limited pulse amplitude and the requirement of linearity of the downconverter. As the fundamental frequency ω_0 is decreased, the tone energy falls even further. Consequently, there exists a minimum tone spacing and a minimum pulse repetition frequency for that the frequency components can still be measured with sufficient accuracy, respectively.

Determination of the Phase Coefficients
The periodic signal which is generated by the HPR can be described in time domain trough a superposition of the particular harmonic components $b_n^{Ref} = \left| b_n^{Ref} \right| \exp j\phi_n^{Ref}$.

$$b^{Ref}(t) = \mathrm{Re}\left\{ \sum_{n=1}^{N} \left| b_n^{Ref} \right| e^{j\left[n\omega_0 t + \phi_n^{Ref} \right]} \right\} \tag{3.13}$$

It must be noted that the measurement starts at the arbitrary and unknown time $t' = t + \tau$ relative to the natural reference t at which the phases ϕ_n^{Ref} have

been defined.

$$b^{Ref}(t') = \text{Re}\left\{\sum_{n=1}^{N}\left|b_n^{Ref}\right|e^{j\left[n\omega_0(t+\tau)+\phi_n^{Ref}\right]}\right\} = \text{Re}\left\{\sum_{n=1}^{N}\left|b_n^{Ref}\right|e^{j(n\omega_0 t+\phi_n')}\right\} \quad (3.14)$$

That results in a modified phase relationship of

$$\phi_n' = \phi_n^{Ref} + n\omega_0\tau \quad (3.15)$$

As shown in figure 3.5, the tones of the HPR can also be described using the incident and reflect DUT waves as well as the complex reflection coefficient Γ_n^{Ref}. Substituting the DUT data by raw measured values in equation 3.2 results in:

$$
\begin{aligned}
b_n^{Ref} &= b_{1,n}^D - a_{1,n}^D\Gamma_n^{Ref} \\
&= \left(\gamma_{1,n}a_{1,n}^M + \delta_{1,n}b_{1,n}^M\right)K_n - \left(a_{1,n}^M + \beta_{1,n}b_{1,n}^M\right)K_n\Gamma_n^{Ref} \\
&= \left[\left(\gamma_{1,n} - \Gamma_n^{Ref}\right)a_{1,n}^M\left(\delta_{1,n} - \beta_{1,n}\Gamma_n^{Ref}\right)b_{1,n}^M\right]K_n \\
&= \tilde{b}_n\left|K_n\right|e^{j\phi_{K,n}}
\end{aligned}
\quad (3.16)
$$

Comparing equation 3.15 and the phase of equation 3.16 results in a system of N equations

$$\phi_n' = \phi_n^{Ref} + n\omega_0\tau = \arg\left(\tilde{b}_n\right) + \phi_{K,n} \quad (3.17)$$

with N+1 unknowns $\{\phi_{K,1}, \phi_{K,2}, ..., \phi_{K,N}, \tau\}$. For the fundamental frequency this equation system reduces to one equation in 2 unknowns:

$$\text{n=1:} \quad \phi_{K,1} = -\phi_1^{Ref} + \omega_0\tau - \arg\left(\tilde{b}_1\right) \quad (3.18)$$

The phase term $\phi_{K,1}$ cannot be resolved, since every LSNA measurement starts at an unknown time τ. However, the phase shift from the DUT ports to the digitizers is not time varying. The consequence is that the phase $\phi_{K,1}$ must be constant from measurement to measurement. Thus, it is possible to define a user defined calibration time reference by setting $\phi_{K,1}$ in equation 3.18 equal to zero:

$$\omega_0\tau = \arg\left(\tilde{b}_1\right) - \phi_1^{Ref} \quad (3.19)$$

Using this calibration time reference, the phase of the harmonic frequencies will be correctly set relative to the fundamental frequency. The remaining phases $\phi_{K,n}$ can now be obtained by:

$$\phi_{K,n} = \phi_n^{Ref} - \arg\left(\tilde{b}_n\right) + n\left[\arg\left(\tilde{b}_1\right) - \phi_1^{Ref}\right], \text{ with } n = \{2, 3, ..., N\} \quad (3.20)$$

It should be pointed out that with the same procedure it is theoretically possible to also perform the power calibration. This implies that also the amplitudes of the HPR tones must be known. However, this method is not yet applied because of missing precisely power characterized HPR generators.

3.4.2   Multitone Phase Calibration

A second approach to generate a multitone signal with known phase relationships is to use an arbitrary signal generator as a multisine source. Here, it is possible to generate a large number of frequency tones with arbitrary phase and amplitude. There are two main differences to the calibration procedure described in section 3.4.1. On the one hand, the tones are located around a center frequency, but need not be equally spaced. On the other hand, the bandwidth of all tones is limited to some tens of MHz, which is dependent of the generators digital to analog converter (DAC) frequency. To obtain an optimum signal to noise ratio (SNR) for the calibration, the amplitudes of every tone have to be maximized, while the LSNA has to be kept within its linear region of operation. Consequently, the crest factor (CF) of the used multitone signal should be minimized (described at the end of this section).

Determination of the Phase Coefficients
In what follows a multisine signal with $N_t = 2N + 1$ tones $b_n^{Ref} = \left| b_n^{Ref} \right| e^{j\phi_n^{Ref}}$ is utilized. An equal carrier spacing $\Delta\omega$ around a center frequency of ω_0 is used:

$$
\begin{aligned}
b^{Ref}(t) &= \mathrm{Re} \left\{ \sum_{n=-N}^{N} \left| b_n^{Ref} \right| e^{j \left[\omega_0(t+\tau) + n\Delta\omega(t+\tau) + \phi_n^{Ref} \right]} \right\} \\
&= \mathrm{Re} \left\{ \sum_{n=-N}^{N} \left| b_n^{Ref} \right| e^{j \left[(\omega_0 + n\Delta\omega)t + (\omega_0 + n\Delta\omega)\tau + \phi_n' \right]} \right\}
\end{aligned}
\tag{3.21}
$$

As in equation 3.14, it applies also here that the calibration measurement starts at a unknown time τ relative to the natural reference. The phases of the particular frequency components are then

$$
\phi_n' = \phi_n^{Ref} + (\omega_0 + n\Delta\omega)\,\tau = \arg\left(\tilde{b}_n \right) + \phi_{K,n}
\tag{3.22}
$$

Again the system of 2N+1 equations cannot be solved without the definition of a user defined time reference. This is obtained by setting the phase $\phi_{K,0}$ of the center frequency to zero and solving equation 3.22 for $\omega_0\tau$:

$$
\text{n=0:} \quad \omega_0\tau = \arg\left(\tilde{b}_0 \right) - \phi_0^{Ref}
\tag{3.23}
$$

Finally, the remaining phases $\phi_{K,n}$ can be calculated:

$$
\phi_{K,n} = \phi_n^{Ref} - \arg\left(\tilde{b}_n \right) + \left(1 + n\frac{\Delta\omega}{\omega_0} \right) \cdot \left[\arg\left(\tilde{b}_0 \right) - \phi_0^{Ref} \right],
$$
$$
\text{with } n = \{-N, -N+1, ..., N-1, N\}
\tag{3.24}
$$

22

Construction of Multitone Signals with Low Crest Factor

Consider a multitone signal $b(t)$ with a periodicity of T as in equation 3.21. The crest factor (CF) of this signal is defined by the ratio of the peak value to its root mean square (RMS) value:

$$\text{CF}\{u(t)\} = \frac{\max |u(t)|}{\text{rms}(u(t))} \tag{3.25}$$

It should be noted that the RMS value is independent of the phase distribution while the peak value dramatically changes with respect to different relative phases of the tones [13]. A signal with equal or equally spaced phases for all tones is the worst expected case and would lead to to crest factors proportional to $\sqrt{N_t}$. A Crest factor proportional to $\sqrt{\log N_t}$ is expected for random phases. That is much smaller but still increasing with the number N of tones.
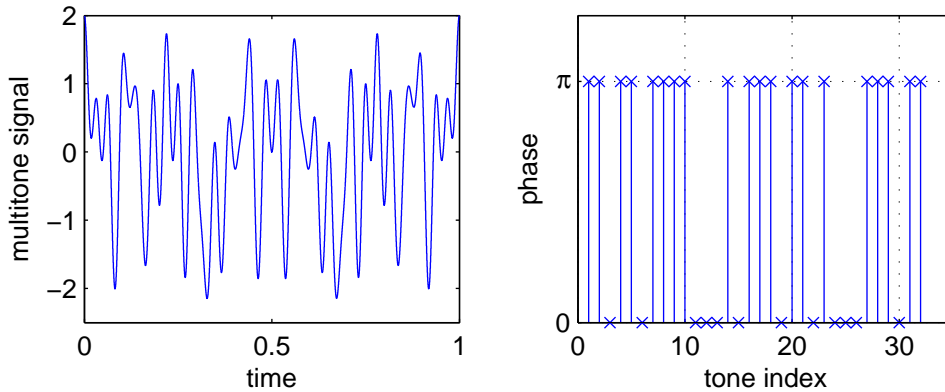
Figure 3.7: 32 tones Shapiro Rudin signal (CF = 6.63 dB)

The literature describes different approaches to minimize the crest factor. In this work, Shapiro Rudin sequences are used to determine the phase ϕ_n^{Ref} [13]. The Shapiro Rudin phases are either 0 or π whereas the amplitudes of all frequency components are equal. Figure 3.7 shows a multisine signal containing 32 tones with the Shapiro Rudin phases relation. The approach has the advantage that phases can very easy be calculated and the resulting signals show reduced crest factors when the number of tones is increased as depicted in figure 3.8. Particularly multisines containing tone numbers equal to the power of two show very low crest factors.
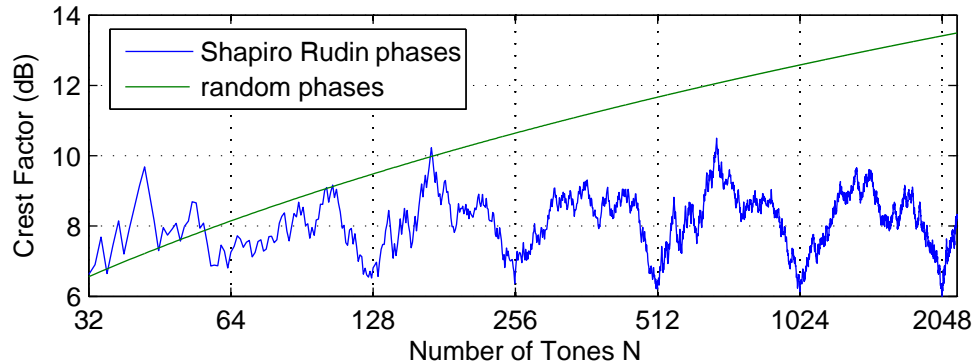
Figure 3.8: Comparison of the Crest factor of Shapiro Rudin type signals and multitoned signals using random phases

3.5 Extension to Broadband Signals

Both methods for phase calibration, described in section 3.4, each have different properties and limits:

- A HPR calibration covers a wide bandwidth. However, due to the limited pulse amplitude, the tone spacing has a lower limit of about $10\,\mathrm{MHz}$.

- Multisines using an arbitrary tone spacing can be generated by an arbitrary waveform generator, but unfortunately the signal bandwidth is limited to some tens of MHz.

This means, that none of the methods can be used individually to calibrate the system for broadband signals with a large number of narrow spaced tones. With the commercialized LSNA, it is possible to measure narrowband modulated signals and their harmonics. The instrument, available to the Institute of Electrodynamics, Microwave and Circuit Engineering, is capable to measure signals with fundamental frequencies above $600\,\mathrm{MHz}$ and modulation bandwidths below $20\,\mathrm{MHz}$ as described in section 1.1. However, for many measurements (e.g. measurements of pulse width modulated (PWM) RF signals), the system must have the capability to measure narrow and equally spaced broadband signals. In literature, some approaches have been proposed to extend the modulation bandwidth to more than twice the IF bandwidth [14], [15], [16]. But so far no method has been described to extend the phase calibration to signals with arbitrarily distributed frequency components. In this section two approaches are described to overcome this restriction with combining different calibration methods.

3.5.1 RF/IF Calibration

This approach, denoted as "RF/IF calibration", uses a separate absolute characterization for the RF and IF path of the system. The main assumption for validity is that the distortions in the RF paths are constant within a small relative bandwidth of about 10^{-3}, which means a constant group delay in this region. The error model of equation 3.2 can be extended to

$$
\begin{pmatrix} a_{1,n}^D \\ b_{1,n}^D \\ a_{2,n}^D \\ b_{2,n}^D \end{pmatrix} = |K_n|\, e^{j\phi_{RF,n}} e^{j\phi_{IF,n}} \begin{pmatrix} 1 & \beta_{1,n} & 0 & 0 \\ \gamma_{1,n} & \delta_{1,n} & 0 & 0 \\ 0 & 0 & \alpha_{2,n} & \beta_{2,n} \\ 0 & 0 & \gamma_{2,n} & \delta_{2,n} \end{pmatrix} \begin{pmatrix} a_{1,n}^M \\ b_{1,n}^M \\ a_{2,n}^M \\ b_{2,n}^M \end{pmatrix} \tag{3.26}
$$

where the relative error coefficient matrix as well as K_n can be determined using a classical relative and absolute power calibration as described in section 3.2 and 3.3. Equation 3.2 assumes equally long IF paths - otherwise the phase distortion $\phi_{IF,n}$ must be replaced by a diagonal 4×4 matrix [17].
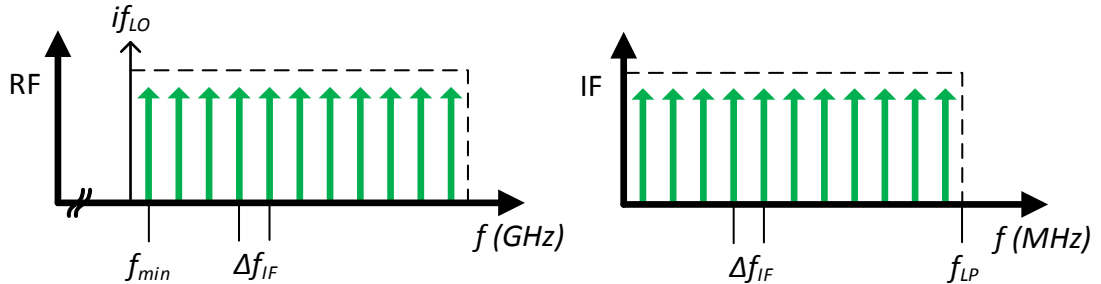
Figure 3.9: IF characterization

The first step of the phase calibration, depicted in figure 3.9 is to characterize the IF phase distortion $\phi_{IF,n}$, caused by the lowpass filter of the downconverter and the transfer characteristic of the ADC. A multisine signal of a bandwidth equal to the IF bandwidth f_{LP} and a minimum frequency f_{min} slightly offset above the LO harmonic if_{LO} is directly applied at channel 1 (cf. figure 3.1). The tone spacing Δf_{IF} must be selected in such a way that the IF transfer function can be interpolated. As shown in figure 3.9, RF frequencies at $f_{min} + n\Delta f_{IF}$ are downconverted to the IF spectrum at $n\Delta f_{IF}$. For a small relative bandwidth of the RF signal, the group RF delay τ_{RF} for all tones is assumed to be constant, whereas a frequency dependent IF group delay τ_{IF} is expected. With a similar approach, as described in section 3.4.2, the relative phase differences of the IF part can be extracted.
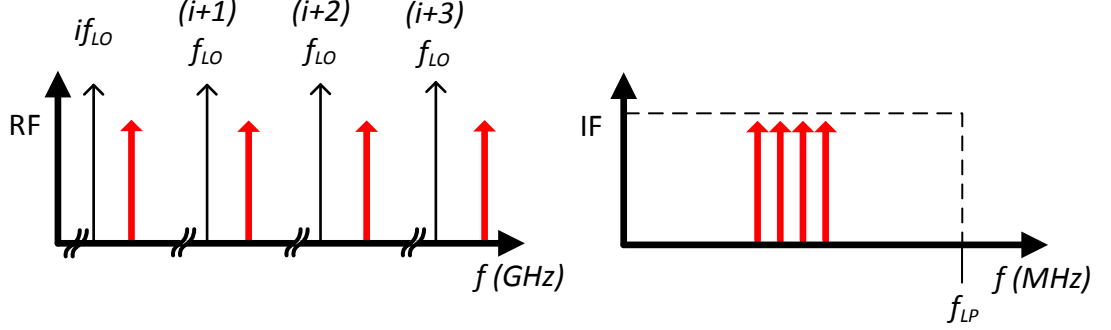
Figure 3.10: RF characterization

The second step, as shown in figure 3.10, is to perform an HPR phase calibration as described in section 3.4.1, with a fundamental frequency in the range of the LO frequency. The IF distortion, also contained in the obtained phase differences can be corrected. Subsequently, the resulting RF phase difference can be interpolated to all measurement frequencies to determine $\phi_{RF,n}$.

Due to many assumptions and the complexity of this method, the multi-tone/HPR combination method was implemented in this work, which is described in the following section.

3.5.2 Multitone/HPR Combination

This method includes a complete characterization of the phase relationships at all measurement frequencies by a relative, an absolute power, and a phase calibration. The core of the concept is the combination of an HPR and multiple multitone calibrations, as shown in figure 3.11.
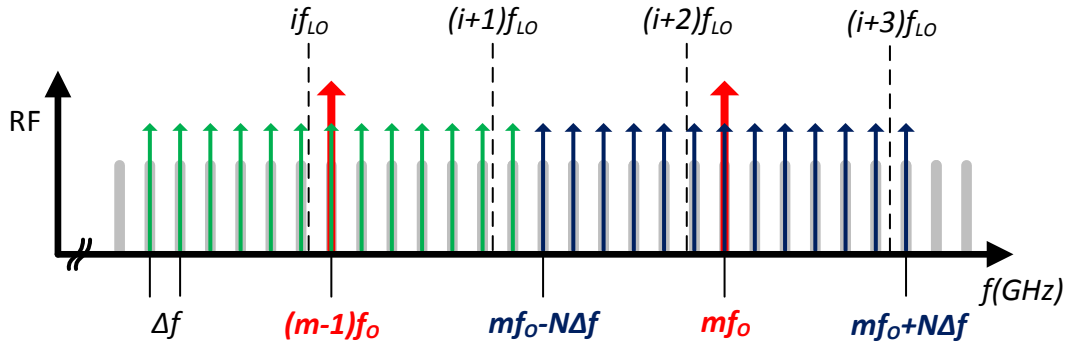
Figure 3.11: Combined multitone/HPR method

An HPR calibration characterizes the phase relationships of M tones $m f_0$

equally spaced over the whole measurement bandwidth subsequently followed again by M multitone calibrations centered around HPR frequencies mf_0 using $2N+1$ tones with a spacing of Δf to cover all measurement frequencies in between the HPR calibration supporting points.

Finally, the phases of all phase calibrations must be correctly aligned as described hereinafter. The only restriction for this method is that the minimum accurately measurable tone spacing of the HPR must be smaller than the maximum multisine bandwidth.

Determination of the Phase Coefficients

Based on the classical HPR calibration, completely equal to the description in section 3.4.1, the phase relationships of all M harmonics at frequencies mf_0 must be computed with following equation:

$$\phi_{K,m}\Big|_{\text{HPR cal}} = \begin{cases} 0, & \text{if } m = 0 \\ \phi_m^{Ref} + m\left[\arg\left(\tilde{b}_0\right) - \phi_0^{Ref}\right] - \arg\left(\tilde{b}_n\right), & \text{if } m = \{2, 3, ..., M\} \end{cases}$$
$$(3.27)$$

Followed by M multitone calibrations, each starting at a random time τ_m. Each calibration measurement results in equation 3.22. Solving the equation for $\phi_{K,m}$ and adapt the nomenclature ($\omega_0 \rightarrow m\omega_0$) results in

$$\phi_{K,m,n}\Big|_{\text{multitone cal}} = \phi_{m,n}^{Ref} + (m\omega_0 + n\Delta\omega)\,\tau_m - \arg\left(\tilde{b}_{m,n}\right)$$
$$= \phi_{m,n}^{Ref} + \left(1 + \frac{n\Delta\omega}{m\omega_0}\right)m\omega_0\tau_m - \arg\left(\tilde{b}_{m,n}\right)$$
$$n = \{-N, ..., -1, 0, 1, ..., N\} \quad m = \{1, 3, ..., M\} \qquad (3.28)$$

to calculate $\tilde{b}_{m,n} = \tilde{b}\left(mf_0 + n\Delta f\right)$, cf. equation 3.16. Because each measurement starts at an unknown time τ_m, it is not possible to solve the equation. However, setting n equal to zero, equation 3.27 and 3.28 can be rewritten:

$$\phi_{K,m}\Big|_{\text{HPR cal}} = \phi_{K,m,0}\Big|_{\text{multitone cal}} = \phi_{m,0}^{Ref} + m\omega_0\tau_m - \arg\left(\tilde{b}_{m,0}\right)$$
$$m = \{1, 3, ..., M\} \qquad (3.29)$$

By determining the unknown

$$m\omega_0\tau_m = \phi_{K,m}\Big|_{\text{HPR cal}} - \phi_{m,0}^{Ref} + \arg\left(\tilde{b}_{m,0}\right) \qquad (3.30)$$

it is possible to completely solve equation 3.28 for all measurement frequencies.

3.6 Re-calculation of the Calibration for Different Attenuator Settings

As for VNA measurements, de-embedding in the context of an LSNA system also means the calculation of the incident and reflected waves at the DUT reference plane from the raw measured values. Once all error coefficients are determined, the de-embedding operation can be simply achieved by computing equation 3.2. Unfortunately, in some applications such as amplifier characterizations, calibration and measurement amplitudes into the system are quite different. In this cases it will be helpful to change the step attenuator settings. Again considering the error model introduced in section 3.1 and the downconverter schematic in figure 2.2, it is found that the error model also contains the transfer characteristics of the step attenuators which it may be described as the result of a multiplication by a $4{\times}4$ diagonal matrix $\mathbf{A}_n$, containing the inverse of the S_{21} parameters from the step attenuators [17].

$$\mathbf{A}_n = \begin{pmatrix} S_{21,att,CH1}^{-1} & 0 & 0 & 0 \\ 0 & S_{21,att,CH2}^{-1} & 0 & 0 \\ 0 & 0 & S_{21,att,CH3}^{-1} & 0 \\ 0 & 0 & 0 & S_{21,att,CH4}^{-1} \end{pmatrix}_n \tag{3.31}$$

The error model for calibration as well as the measurement can be described by

$$\text{calibration}: K_n \begin{pmatrix} 1 & \beta_1 & 0 & 0 \\ \gamma_1 & \delta_1 & 0 & 0 \\ 0 & 0 & \alpha_2 & \beta_2 \\ 0 & 0 & \gamma_2 & \delta_2 \end{pmatrix}_{n,CAL} = \mathbf{T}_{n,CAL} = \tilde{\mathbf{T}}_n \cdot \mathbf{A}_{n,CAL} \tag{3.32}$$

$$\text{measurement}: K_n \begin{pmatrix} 1 & \beta_1 & 0 & 0 \\ \gamma_1 & \delta_1 & 0 & 0 \\ 0 & 0 & \alpha_2 & \beta_2 \\ 0 & 0 & \gamma_2 & \delta_2 \end{pmatrix}_{n,MEAS} = \mathbf{T}_{n,MEAS} = \tilde{\mathbf{T}}_n \cdot \mathbf{A}_{n,MEAS} \tag{3.33}$$

The transfer matrix $\tilde{\mathbf{T}}_n$ contains all distortions from the system except the step attenuators response. Knowing the S_{21} parameters of the step attenuators, $\tilde{\mathbf{T}}_n$ can be re-calculated by $\mathbf{T}_{n,CAL}^{-1} \cdot \mathbf{A}_{n,CAL}$. Consequently, the frequency components at the DUT ports can be retrieved from

$$
\begin{pmatrix} a_{1,n}^D \\ b_{1,n}^D \\ a_{2,n}^D \\ b_{2,n}^D \end{pmatrix} = \mathbf{T}_{n,MEAS} \begin{pmatrix} a_{1,n}^M \\ b_{1,n}^M \\ a_{2,n}^M \\ b_{2,n}^M \end{pmatrix} = \mathbf{T}_{n,CAL} \cdot \mathbf{A}_{n,CAL}^{-1} \cdot \mathbf{A}_{n,MES} \begin{pmatrix} a_{1,n}^M \\ b_{1,n}^M \\ a_{2,n}^M \\ b_{2,n}^M \end{pmatrix} \tag{3.34}
$$

Chapter 4

Characterization of the N4464A Sampling Downconverter

As already mentioned in section 1.1, the documentation of the Agilent Technologies N4464A sampling downconverter became public domain. It consists of schematics of an HP MTA which is an integral part of the LSNA and a description of the PC104 system inside the N4464A. Also included are the high and low level standardized commands for programmable instruments (SCPI commands) which can be used to control all components as depicted in figure 2.2. This allows to setup an LSNA using the sampling downconverter as "core" of the system. To get a deeper understanding of the downconverter hardware, it will be necessary to characterize the instrument and test the components inside. Some SCPI commands are sparsely described and their functionality cannot be recognized from the command name. Consequently, it is also necessary to test these commands and investigate their meaning in some kind of reverse engineering.

It should be noted, that the principal aim of this characterization is not to measure the LSNA precisely, e.g. obtain transfer functions of some components, rather it is the determination of fundamental properties, possibilities, and limits of the system. As a result of these measurements it was possible to define power limits, minimum tone spacings, or principle transmission characteristics over a certain bandwidth. Based on the LSNA system manual [18], the existing specifications have been verified and later on modified and extended into a more detailed specification which can be found in appendix A.

4.1 Measurement Setup Overview

In order to characterize the downconverter, a test system as shown in figure 4.1 was set up which contains the four channel downconverter as DUT, whereby each channel can be measured individually. A microwave source generates an RF test signal, which is downconverted to the IF bandwidth. A power meter, that receives the same amount of power as the downconverter, is used to determine the input power.
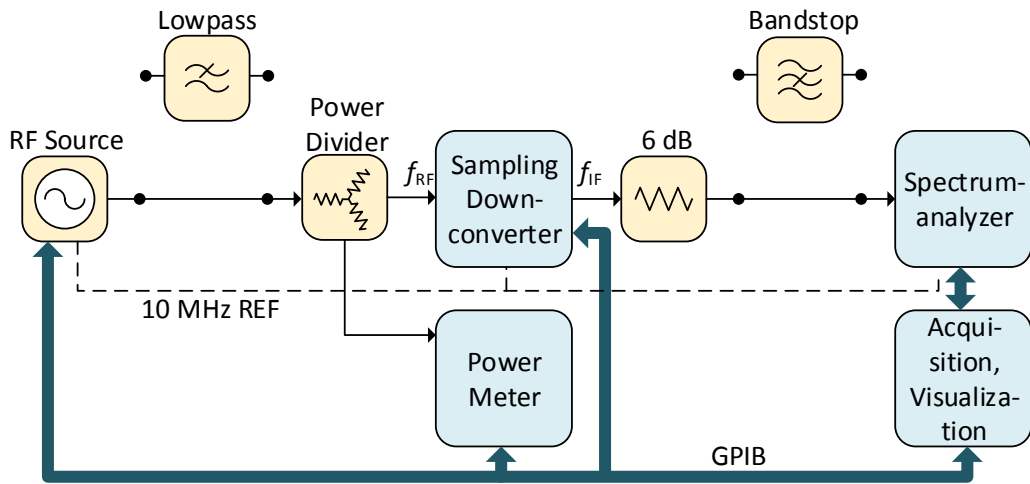
Figure 4.1: Downconverter characterization measurement setup

All instruments are connected to a PC using a general purpose interface bus (GPIB) to USB interface. In this work, Matlab in combination with the Instrument Control Toolbox has been used to communicate to the instruments, to acquire data, and to visualize the results.

Depending on the frequency settings of f_{RF} and f_{LO}, either RF sweeps with constant IF frequency or sweeps over the whole IF bandwidth at nearly constant relative RF frequencies can be obtained. Power sweeps can be realized by variations over RF source power, attenuator, or amplifier settings. The lowpass and the bandstop filter at top line in figure 4.1 can be inserted to suppress unwanted source harmonics or downconverter mixing products.

4.2 Measurements

Various test measurements have been conducted to characterize the downconverter. Different settings of the components inside the LSNA, as depicted in

figure 4.2, have been tested. For example, measurements with various local oscillator frequencies f_{LO}, step attenuator settings l_{att}, and amplifier settings g_{amp} have been performed. Some settings of the initially undefined parameter "RC-FILTers" n_{RC} have been utilized to investigate the meaning of the parameter. Together with sweeps over the input frequency f_{RF} and input power P_{in}, a deeper insight in the downconverter behavior was gained. The most interesting measurements and results are described in what follows.
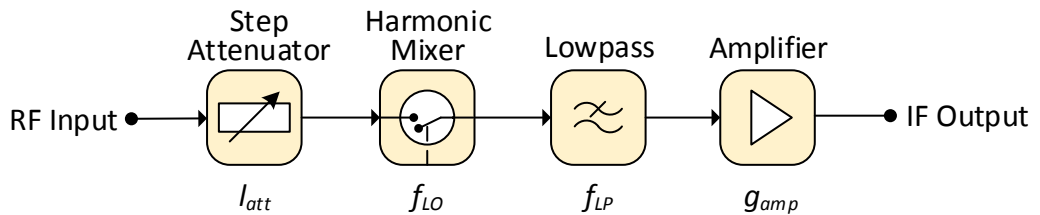
Figure 4.2: Main components of a single channel of the downconverter

4.2.1 Linearity/Compression

As already mentioned in section 3.1, the LSNA can be described using linear models as long as a certain amplitude at the RF input is not exceeded. For that reason, several measurements with various input powers and amplifier settings were made. To get a first impression of the transfer characteristic, particular at higher input powers, the measurement as depicted in figure 4.3 has been performed. The figure shows a sweep of the input power using all possible gain settings $g_{amp} = 0,6,...,36\,\mathrm{dB}$, while the output power is measured. The RF and LO frequencies have been adjusted in such way that the signal at the IF output is located at 1 MHz. For all measurements, the maximum input power has been determined to smaller than 0 dBm. This refers to the "Operating Range" and is 10 dB smaller than the "Damage Level", that can be found in the system manual [18]. The utilized measurement setup is based on figure 4.1, neither containing the lowpass nor the bandstop filter.

The upper part of figure 4.3 displays the measured output power while the lower part shows linearity error, the differences in relation to a perfect linear relationship. It can be seen that all curves are almost ideal up to an input power of –20 dBm. In regard to the other small variations of about 0.1 dB, no further exact statement can be made, because it also contains inaccuracies from the power meter and the spectrum analyzer. However, by selecting gains of 30 and 36 dB, it can be seen clearly that the amplifier gets into compression at about –18 dBm, and respectively –12 dBm input power. From this measurement it can be clearly

seen that the input power at these amplifier settings must be limited far below the "Operating Range".
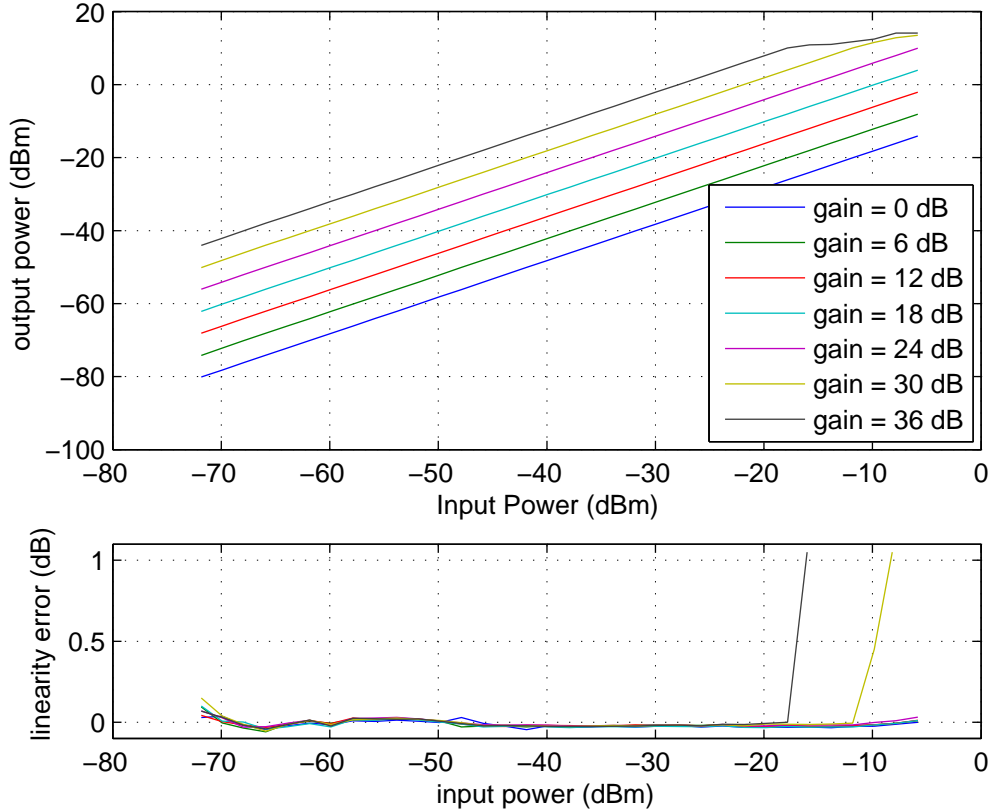
Figure 4.3: Linearity of the downconverter. $l_{att} = 0\,\mathrm{dB}$, $f_{RF} = 1.801\,\mathrm{MHz}$, $f_{LO} = 20\,\mathrm{MHz}$

In order to get a better understanding of the non-linear behavior of the down-converter, further measurements were made, containing the output power at the fundamental frequency as well its higher harmonics. To acquire the power at the fundamental frequency, the measurement setup is exactly the same as above. However, the higher harmonics at the IF output are smaller by several orders of magnitude compared to the fundamental. To achieve a high dynamic range, while prevent an overload at the spectrum analyzer input, a 1 MHz bandstop was built and inserted in this measurement (cf. bandstop in figure 4.1).
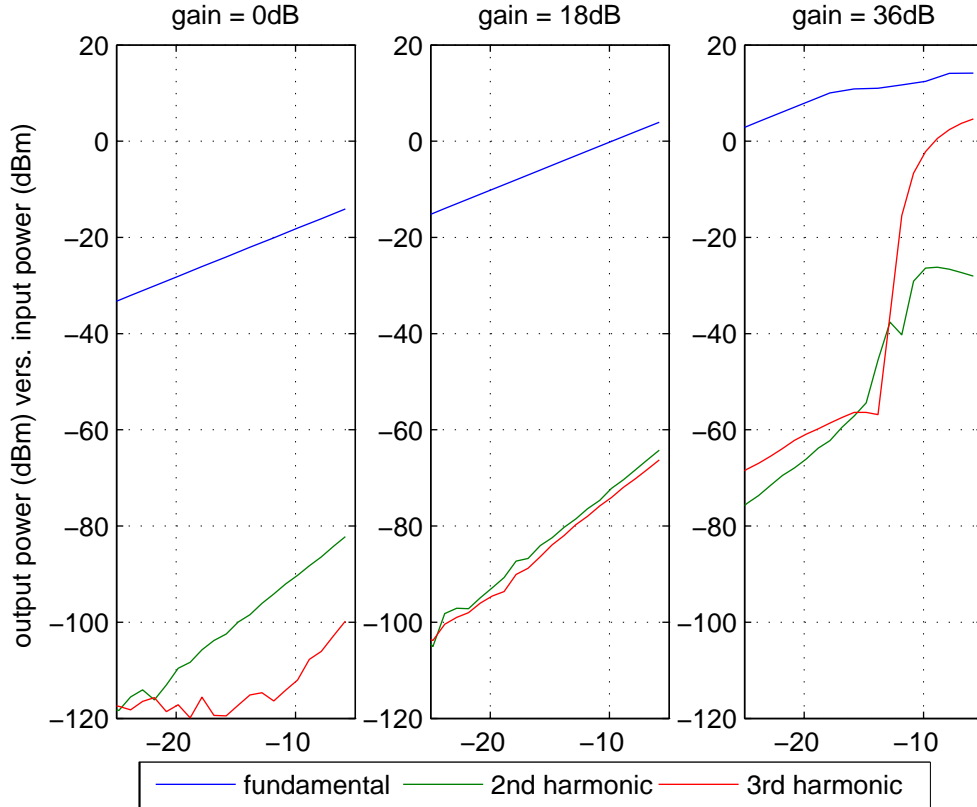
Figure 4.4: Output of fundamental and harmonics versus input power. $l_{att} = 0\,\text{dB}$, $f_{RF} = 1.801\,\text{MHz}$, $f_{LO} = 20\,\text{MHz}$

The ratio of a fundamental signal to the highest spurious signal is defined as the spurious free dynamic range (SFDR). The results of this measurement are displayed in figure 4.4 also depicts the it corresponds to the difference of the fundamental to the maximum of the 2nd and 3rd harmonics in the dB scale. A SFDR of 70 dB at input powers below –10 dBm and a gain setting of 0 dB could be determined which is in the same order of magnitude as frequently found in literature [1].

4.2.2 RF/IF Frequency Response

Characterization of the transfer characteristics of the downconverter at RF and IF frequencies were done by several sweeps and is described in what follows. All measurements have been performed using the setup as depicted in figure 4.1 without the use of the additional filters.

RF Characterization

The RF bandwidth of the N4464A sampling converter is specified from DC up to 50 GHz [18]. However, it would be helpful, to know the transfer characteristics of the RF part, for example, to get a better understanding of the frequency dependent dynamic range.
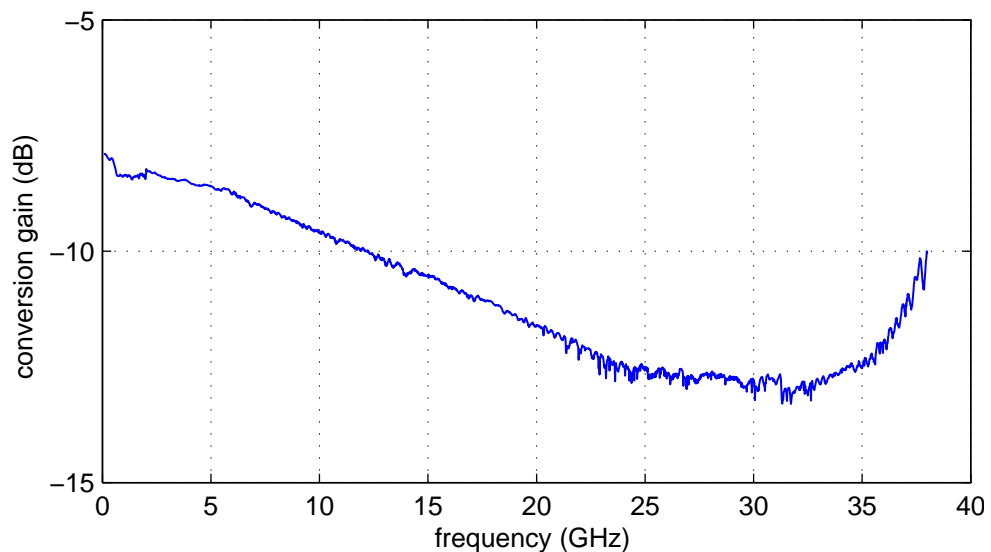
Figure 4.5: RF transfer characteristic. $l_{att} = 0\,\mathrm{dB}$, $f_{LO} = 20\,\mathrm{MHz}$, $g_{amp} = 0\,\mathrm{dB}$

To perform this measurement, the input frequency was swept over a wide bandwidth while keeping the mixing products at a constant position. For example the local oscillator frequency is set to 20 MHz and the RF frequency grid starting at 99 MHz and using a tone spacing equivalent to the LO frequency of 20 MHz, leads to mixing products that are located at 1 MHz for all RF frequencies. Each individual input frequency mixes with another LO harmonic as described in section 2.1.1. Consequently, the resulting transfer characteristic consists of the frequency dependent losses within the RF part in conjunction with the frequency dependent spectral response of the sampling pulses. The measurement results, depicted in figure 4.5, show the conversion gain up to a frequency of 38 GHz containing a tolerable frequency dependence of about 5 dB.

IF Characterization

As shown in figure 4.2, the frequency dependent components of the IF part mainly include the lowpass filter and the amplifier. Sweeping over a small relative RF bandwidth from 1.8 to 1.85 GHz at a LO frequency of 20 MHz, causes a sweep over

the whole IF bandwidth. Under these circumstances, the frequency dependence of the RF part can be largely neglected.
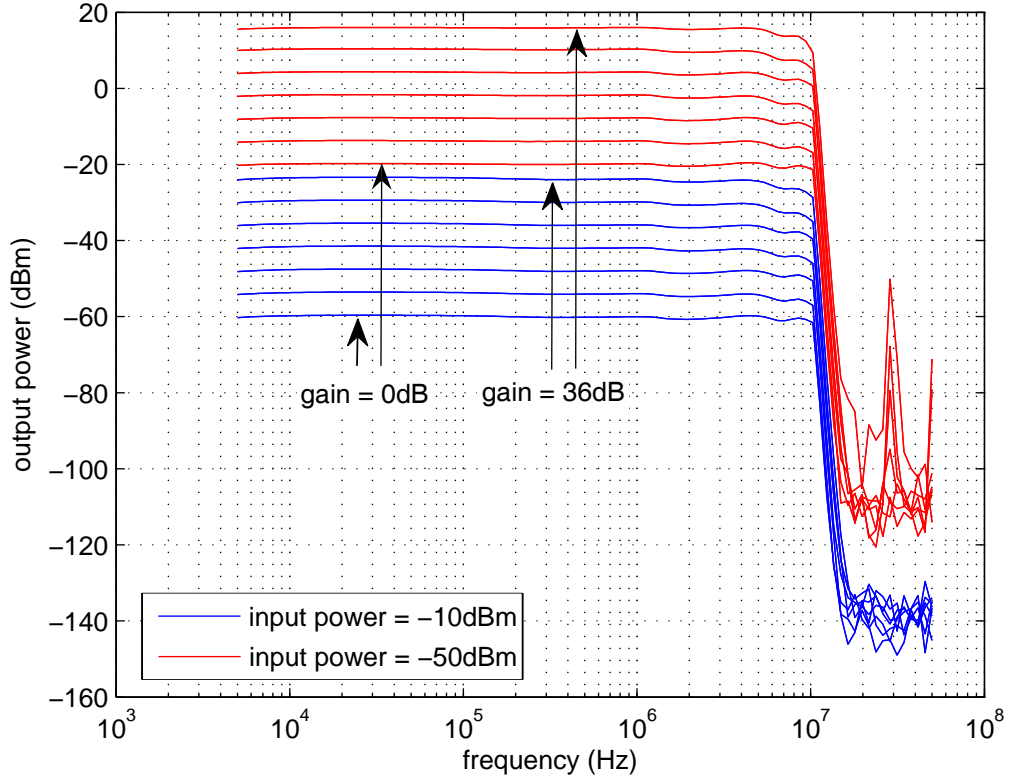
Figure 4.6: IF transfer characteristic. $f_{RF} = 1.8 - 1.85\,\mathrm{GHz}$, $l_{att} = 0\,\mathrm{dB}$, $f_{LO} = 20\,\mathrm{MHz}$, $g_{amp} = 0,6,...,36\,\mathrm{dB}$

The measurements where performed using all amplifier settings and various input powers, as depicted in figure 4.6. They show a relatively flat response over the entire IF bandwidth with minor amplifier dependent changes. Additionally, the stop band attenuation of the IF filter can be determined to larger than 80 dB at 12.5 MHz which allows to use ADCs with a sampling frequency of about 25 MHz. The discrepancies on the four upper most red curves at about 30 MHz correspond to RF input frequencies of 1.83 GHz can be explained as follows: The input signal mixes also with the LO harmonics at 1.82 and 1.84 GHz which leads to IF frequencies each at 10 MHz. Based on the measured observations, the assumption arises that constructive interference causes the amplifier to operate in its highly non-linear region, resulting in third order harmonics, again at 30 MHz.

Investigation of the "RC Filters" Value

As already mentioned, the meaning of the SCPI-command "DOWNConverter:RCFILTers" cannot be recognized from its name or the description "set/ask the value of RC compensation filters" in the SCPI command overview. The value consists of one byte, which can be set individually for each channel. Each bit is a "stage that can be switched in" [19].
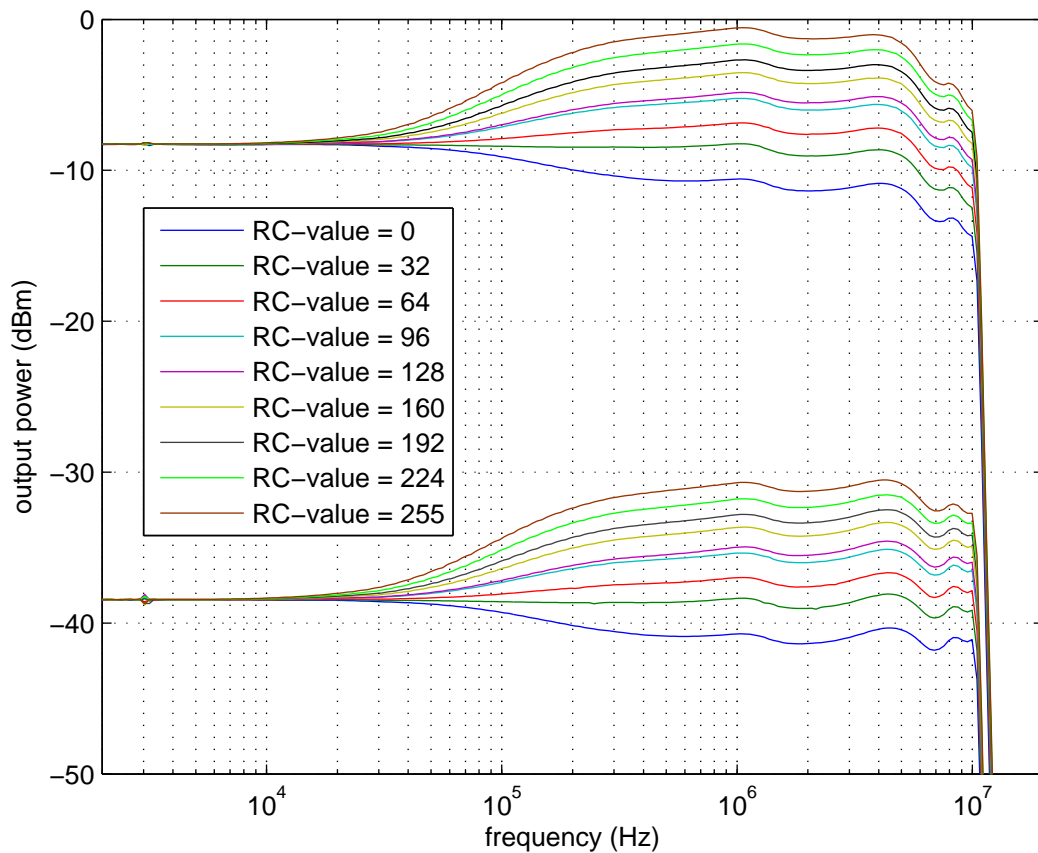
Figure 4.7: RC Filter value effects. $g_{amp} = \{0, 30\}$ dB

The test to investigate this command was conducted in the same manner as the IF characterization above. As depicted in figure 4.7, the setting of the parameter of this command changes the frequency response between very low and higher IF frequencies which also depends on the gain settings. The signal analyzer which the LSNA is based of consists of a split-band amplifier [20]. Therefore, it was concluded that the value of this parameter corresponds to the setting of a shaping amplifier, in order to obtain a best achievable flat frequency response between both paths.

4.2.3   Phase Noise

Under the assumption of ideal sampling pulses, as discussed in section 2.1.1, it will theoretically be possible to compress infinite frequency components from the RF input into the IF bandwidth. However, also this ideal compression will get impossible due to the fact that the higher the frequency resolution, the higher the number of recorded samples are limited because of storage limits. In practice, the number of tones in the IF bandwidth will already be limited due to significant bandwidths of each individual tone due to phase noise.
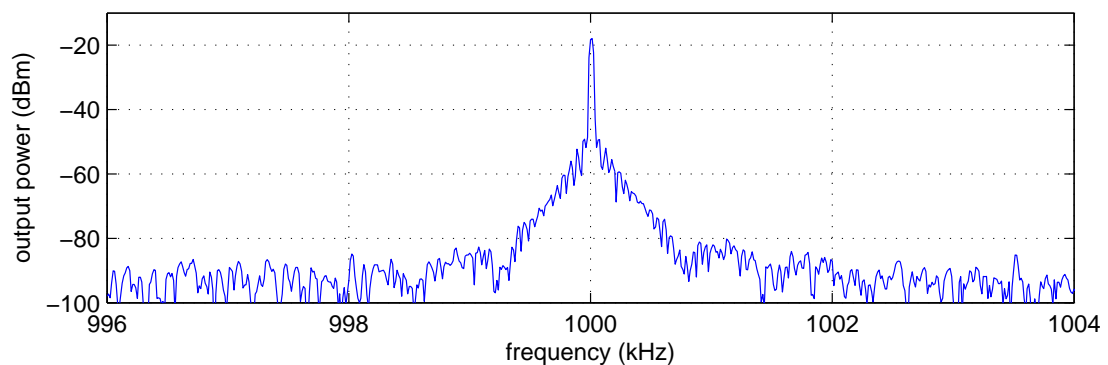
Figure 4.8: Phase noise at the IF output. $f_{RF} = 501\,\text{MHz}$, $f_{LO} = 20\,\text{MHz}$, resolution bandwidth (RBW) $= 30\,\text{Hz}$

At all measurements a sporadically broadening of the IF output spectrum was observed. Figure 4.8 shows the frequency spectrum at the IF output which contains one single tone that was mixed down from $501\,\text{MHz}$ to $1\,\text{MHz}$ using a LO frequency of $20\,\text{MHz}$. Phase noise broadens the tone to about $1\,\text{kHz}$, at $60\,\text{dB}$ below the carrier. This fact is not unexpected since the measurement is consistent with the information that can be found in the specifications [18]. Nevertheless, it is confusing that the shape of the spectrum changes dramatically over time. For many seconds up to minutes, the bandwidth $60\,\text{dB}$ below the carrier is less than $500\,\text{Hz}$ after which it changes back to the depicted behavior. This behavior has been observed at many different downconverter settings, different input powers and frequencies as well as different $10\,\text{MHz}$ reference sources. Utilizing a spectrum analyzer measurement, no statement could be made about the reason of this behavior, especially of the time dependent effect.
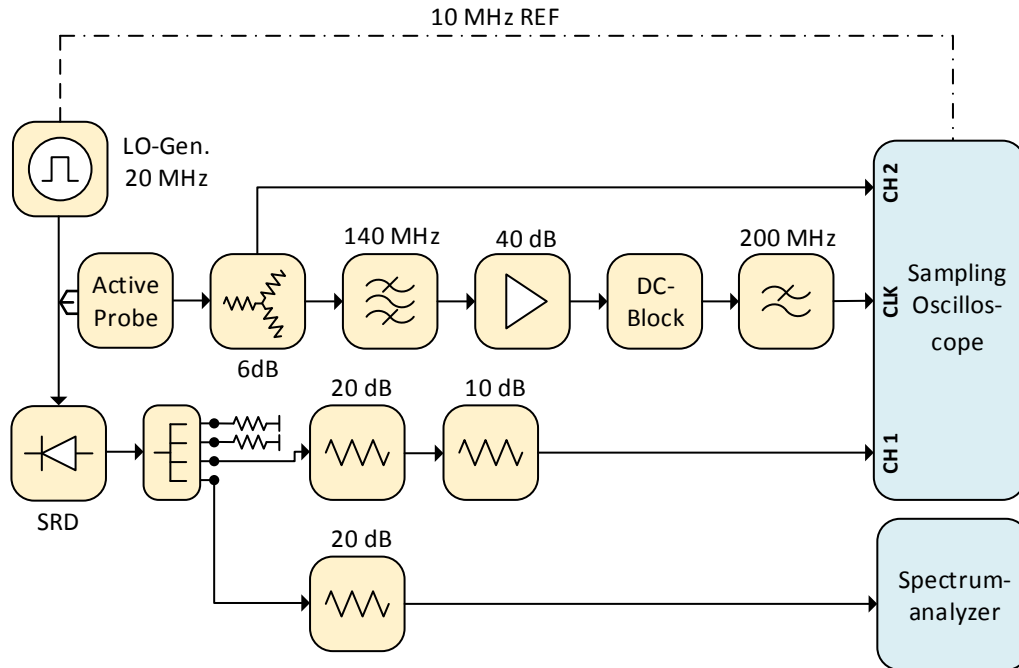
Figure 4.9: Jitter measurement setup

Consequently, a measurement setup which is illustrated in figure 4.9 was built due to further investigation of this effect. The measurement goal was to observe the time dependent jitter of both the SRD output and the fractional-N synthesizer output, that are connected to channel 1 and channel 2 of the sampling oscilloscope which is set to the coherent interleaved (CIS) sampling mode. This mode is used exclusively to measure jitter because it uses the signal applied to the CLK/Prescale input as a reference for an internal phase locked loop (PLL) [21]. It turned out not to be possible to directly trigger by the rectangle pulse of the synthesizer because of a minimum required input frequency of 125 MHz for the CIS timebase mode. Therefore, a cascade of filters was inserted to obtain the seventh harmonics of the LO rectangle pules at 140 MHz. It must be noted that it can only be triggered at every seventh edge because it takes seven periods of the trigger signal to obtain one measurement signal period. The whole test setup contains several switched in attenuators and amplifiers in order to obtain appropriate signal levels.
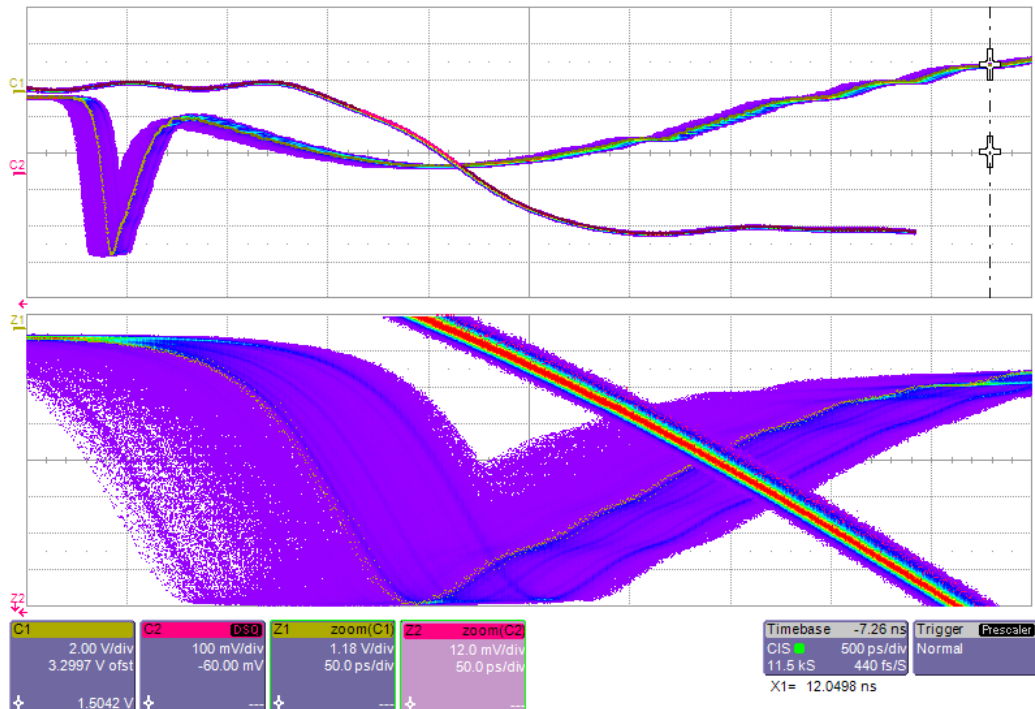
Figure 4.10: Jitter measurement between synthesizer and SRD output

Both signals have been measured in analog persistence mode which accumulates on-screen points from many acquisitions to see signal changes over time. Figure 4.10 depicts the falling edge of the synthesizer together with the SRD output pulse for a 5 minutes measurement time. The falling edge is relatively stable over the whole time whereas the pulse contains a considerable jitter. Additionally, the same random time dependent behavior could be determined as for the spectrum analyzer measurement. Sometimes the falling edge of the pulse was almost constant up to a minute. Based on all these measurement results it can be assumed that the step recovery diode is responsible for the phase noise effects at the downconverter output. Further investigation, for example a better stabilization of the SRD power supply did not bring any enhancements. Consequently, negative influences based on this effect can only be avoided by limiting the tone spacing at the RF input as well as at the IF output to 1 kHz.

4.2.4   Step Attenuator

The N4464A downconverter contains programmable attenuators which can be set individually for each channel from 0 to 60 dB in 10 dB steps. It consists of three stages with 10, 20, and 30 dB attenuation. After a power up or an initialization command for the step attenuator subsystem (STEPAT:INIT), the attenuators are set to the maximum attenuation value for each channel.

Various measurements have been performed at different RF frequencies, at all channels, for all possible attenuator settings. During these tests, no irregularities have been detected. It is worth mentioning that changes in the attenuator settings, performed by the PC104 system inside the downconverter, are made in a special way. First, all necessary stages will be activated before any stages are removed which prevents the sampler from overload between the switching operations. For example, increasing the attenuation value from 20 to 30 dB causes a sequence of $20\,\text{dB} \rightarrow 50\,\text{dB} \rightarrow 30\,\text{dB}$.

Chapter 5

LSNA System for Arbitrary Periodic Signal Measurements

It was the main objective of this work to develop an LSNA system for broadband measurements of periodic signals. Using the commercialized system, the user has different choices to get access to the LSNA functionality. A Mathematica interface allows full control, whereas the control graphical user interface (GUI) only allows basic control [22]. It turned out to be more convenient to directly control the functionality of the LSNA using its GPIB interface utilizing SCPI commands. Therefore, during this thesis a measurement system was built that contains all essential components of an LSNA (source, test set, downconverter, acquisition, processing) as shown in figure 5.1. The complete software implementation including instrument control, data acquisition as well as data processing has been done utilizing Matlab and its Instrument Control Toolbox.

The following sections contain a summary of guidelines that must be fulfilled at a broadband LSNA, a detailed description of the built measurement system, as well as the measurement procedure itself. Finally, some measurements are presented that verify the implemented calibration.

5.1   Design Guidelines

Before starting an LSNA measurement, one must consider some requirements to make precise calibrated measurements. The following summarizes all these guidelines regarding to input signals, frequency, and power settings.

Periodic Signals
The strongest requirement for the realized setup is that the RF input signal must

be periodically with some period of time T_{RF}. This is because the LSNA consists of a harmonic mixer that mixes the RF signal down to IF according to the harmonic sampling principle. As presented in section 2.1, this harmonic principle can only be applied to periodic signals.

Power Constraints
Calibration and thus also the measurement error correction assumes a linear system behavior which is sufficiently fulfilled up to a certain power level at the RF input (described at section 3.1). Consequently, the power that is fed into the downconverter inputs must not exceed the limits in appendix A.2, that also depend on settings of the downconverter. However, to reach the maximum achievable dynamic range, the downconverter's output power, especially during the calibration, should be adjusted in such a way to make full use of the dynamic range of the ADC.

Calibration
Without a calibration, the measured raw data of all four channels is almost meaningless. Pre-defined standards for the whole measurement bandwidth must be available in order to carry out a calibration as discussed in chapter 3.

LO Settings
The local oscillator frequency f_{LO} must be selected in such way that the tones downconverted to IF are not overlaid. An optimum use of the IF bandwidth which refers to equally spaced IF frequency components leads to a maximum possible measurement dynamic range as already described in detail in section 2.1.

ADC Settings
In order to perform coherent digitizing, the discrete Fourier transform (DFT) frequencies of the measured signals must be exactly aligned to the frequency components of the IF signal. Therefore, the acquisition time $T_{acquire}$ and the number of samples N_{ADC} within this time can be selected in the presented system. Coherence can be achieved by setting the sampling time $T_{acquire} = N_{ADC}/f_{ADC}$ equal to an integer multiple of the IF period $T_{IF} = 1/\gcd\left(f_{IF,n}\right)$, where $\gcd(f_{IF,n})$ denotes the greatest common divisor of all IF tone frequencies [23]. Consequently, the number of samples can be determined by

$$N_{ADC} = m \cdot \frac{f_{ADC}}{\gcd\left(f_{IF,n}\right)} = m \cdot f_{ADC} T_{IF}, \quad m \in \mathbb{N} \tag{5.1}$$

Well Defined Measurement Times
The system contains a time reference generator which produces trigger pulses at f_{trig} to start the recording of the IF signal. In order to get equal conditions and equal phase relationships between multiple measurements and for calibration and measurements, respectively, some requirements regarding the trigger pulse must furthermore be satisfied. The trigger period $T_{trig} = 1/f_{trig}$ must be an integer multiple of

- the IF period $T_{trig} = n_1 \cdot T_{IF}$,

- the local oscillator period $T_{trig} = n_2 \cdot \frac{1}{f_{LO}}$,

- and the ADC acquire time $T_{trig} = n_3 \cdot \frac{N_{ADC}}{f_{ADC}} = n_3 \cdot T_{ADC}$,

where $n_1, n_2, n_3 \in \mathbb{N}$ [10], [14]. If a trigger frequency satisfies these conditions, the phase relationships of subsequent measured signals are equal.

5.2   System Overview

Figure 5.1 shows the LSNA system that was built in this work. It consists of some building blocks using the Agilent N4464A downconverter as main component. The hardware setup and the communication to the instruments is described in what follows.

5.2.1   Hardware Setup

In contrast to the generic LSNA shown in figure 2.9, the LSNA system that is depicted in figure 5.2 implies several differences.

The test set simply consists of two directional couplers, which sense the incident and reflected waves from the DUT test ports. On the one hand this is an advantage because there are no switches in the system, for example, to feed in the RF signal from the port 1 or port 2 side. A switch would introduce cross-coupling that is not taken into account in the error model as discussed in section 3.1. On the other hand, some re-connecting has to be made during the calibration which takes additional time and could also have negative influence to the quality of the calibration, because the error model assumes equal source impedances at the calibration and measurement.

A four channel oscilloscope is utilized to acquire the raw measured data and transmits the recording to a PC system. It turned out that the transfer rate for larger amounts of data is approximately equal for a USB and a local area network (LAN) connection. Consequently, the oscilloscope was directly connected to an
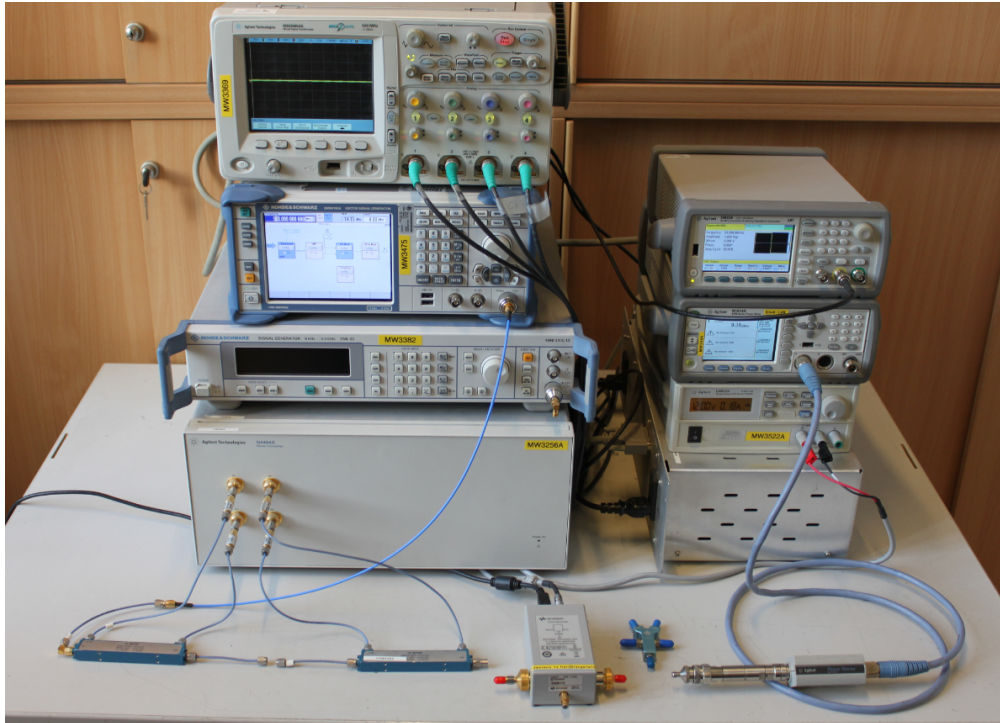
Figure 5.1: Developed LSNA system

USB port at the PC. The measurement is triggered by a pulse of a time reference generator whose frequency f_{trig} is adjusted according to the guidelines presented in section 5.1. The RF signal generator has various functionalities in this system, which can all be carried out using one device. At the relative and absolute power calibration, the generator is utilized as continuous wave (CW) RF source (figure 5.4 a – d) whereas it generates the reference input signal at the HPR calibration (figure 5.4 e). During the multitone calibration it is connected directly at a DUT port and generates a multisine with known phase relations (figure 5.4 f).

Figure 5.2 also shows that all instruments are connected via the GPIB or USB interface, either directly at a standard PC system, or to a USB to GPIB converter, that is connected to the PC. The oscilloscope, the downconverter, and the trigger generator are supplied by the same 10 MHz reference frequency which is provided by the RF signal source. Either the used instruments and components utilized SMA compatible connectors or they are connected to adapters so that it was possible to use SMA coaxial cables for all RF signals. The connection between the downconverter and the oscilloscope, the reference generator and the oscilloscope, as well as all 10 MHz reference connections are established using BNC cables. A detailed listing of all used components and instruments can be found in table 5.1.
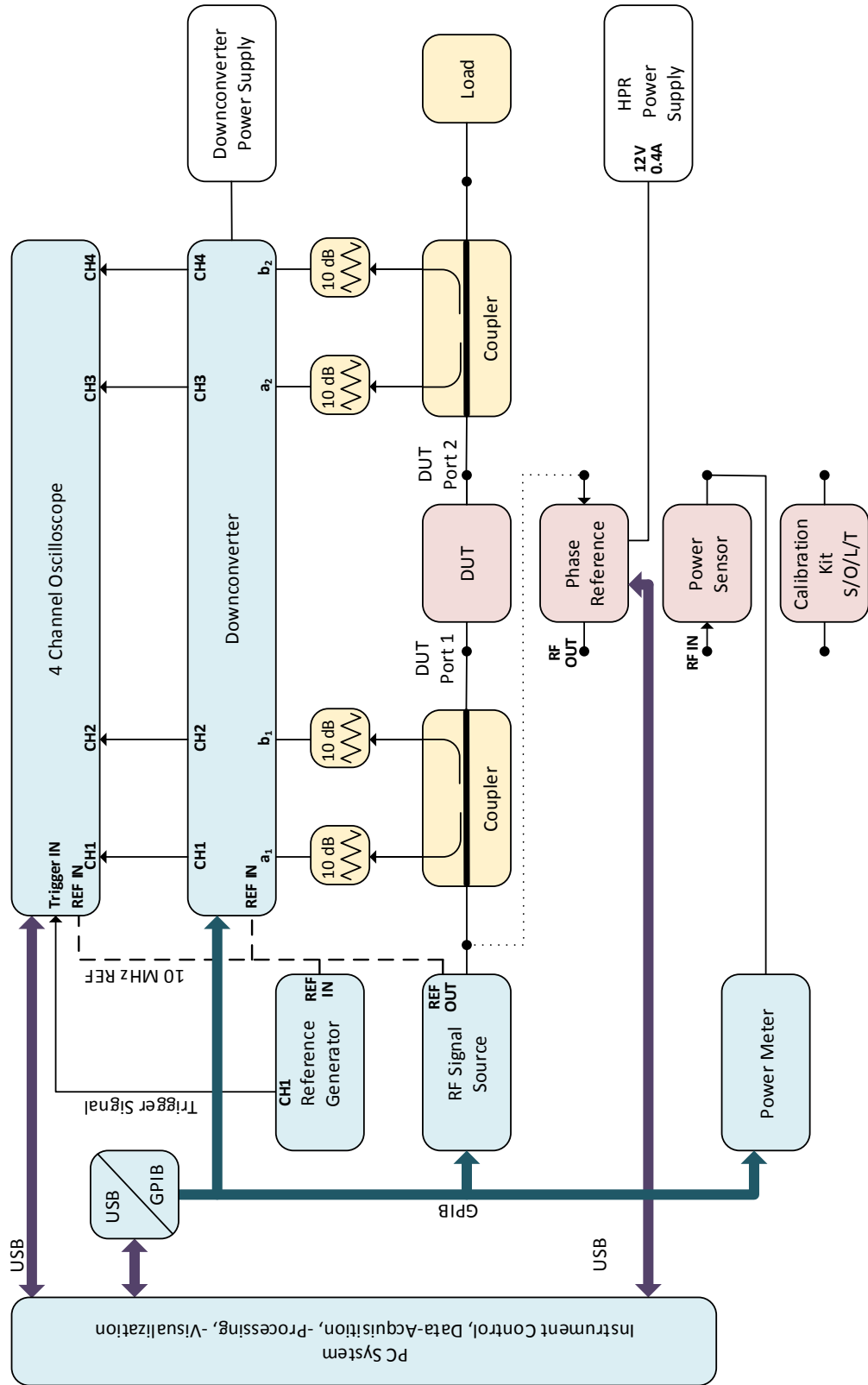
Figure 5.2: Block diagram of the developed LSNA system

Instrument	Type	Characteristics
Downconverter	Agilent N4464A	$DC - 50\,\text{GHz}$
Vector Signal Source	R&S SMBV100A	$9\,\text{kHz}$ to $6\,\text{GHz}$
RF Signal Source	R&S SML03	$9\,\text{kHz}$ to $3.3\,\text{GHz}$
Oscilloscope	Agilent MSO6054A	4 Channel
Power Meter	Agilent N1914A	
Power Sensor	Agilent E9300H	$10\,\text{MHz} - 18\,\text{GHz}$
Trigger Generator	Agilent 33522A	Square, 1 Vpp
Phase Reference	Keysight U9391F	$10\,\text{MHz} - 50\,\text{GHz}$ char.
Phase Ref. Power Supply	Agilent U8992A	12 V, 0.5 A lim.
Directional Coupler	$2 \times$ Krytar 1850	$0.5 - 18\,\text{GHz}$
Calibration Kit	R&S ZV-Z132	3.5 mm m/f

Table 5.1: LSNA system components

5.2.2 Instrument Control

Generally, the communication is accomplished utilizing the functions contained in the instrument control toolbox of Matlab. An exception is the phase reference which is controlled using "libusb-1.0.19", a C library that gives applications easy access to USB devices on many different operating systems [24]. "libusbK", version 3.0.7.0 is the currently installed generic driver for vendor class USB device interfaces [25]. The HPR can be simply activated by executing a short program written in C, that sends two commands at an interrupt transfer and reads the acknowledgements from the HPR. The first one-byte command 0x06h initializes the phase reference and turns the output on. After this, the second command 0x0Ch sets a divider of 16. This means that the pulse repetition frequency equals one sixteenth of the HPR input frequency. An overview of all known commands is given in appendix B.

For all other instruments, classes have been implemented in Matlab which support establishing a connection and contain necessary functions to operate the LSNA. The following describes the classes and their most important functionalities.

Downconverter Class "*lsna*"
Defining an *lsna* object establishes a GPIB connection and initializes the downconverter using specified or default settings. The minimum number of arguments

at the definition contains only the GPIB board index and the GPIB address. The properties of the *lsna* class cover all features of the components inside, such as attenuator, gain, coupling, DC offset, or local oscillator settings. All these properties can be set (if necessary, individually for each channel) at the downconverter. There also exist some functions to retrieve information about status bytes or event registers, to map these numbers to their meaning, and to further display them. Additionally, there is a function that performs an automatic DC offset zeroing which is recommended to be executed after initialization and after amplifier settings modifications.

Oscilloscope Class "*scope*"
This class has been implemented for the Agilent MSO6054A mixed signal oscilloscope. The connection can be established via USB or LAN, only the VISA address of the device must be known. A *scope* object contains some default properties suitable for digitizing the IF output signal of the downconverter, for example channel, acquire, timebase, trigger, or waveform settings. Properties that can be defined and set by the user, are only the acquisition time and the number of recorded samples. Potential settings can be found in [26]. All default and user defined properties will also be set at an initialization, that is executed after the definition of a *scope* object. The most important function during the calibration or a measurement is the "acquire" function which reads the waveform of the selected channels. Finally, it returns the measured data in frequency domain together with a vector of contained frequencies which is calculated utilizing the properties contained in the object.

Vector Signal Generator Class "*smbv*"
An *smbv* object must be defined by its GPIB board index and the GPIB address. This class only contains functions, that are needed to use the generator as a source in an LSNA system. For example, to set the output power, the frequency, or to turn the output on/off. Besides these, it is possible to easily create multitones by using the arbitrary waveform generator. The arguments of the corresponding function "mode_arb" are output power, carrier frequency, and the inphase/quadrature (IQ) data.

Power Meter Class "*powermeter*"
The power meter is just used during the absolute power calibration. Therefore, the class only supports acquiring of power at a desired frequency, measured by a power sensor. After defining a *powermeter* the user is asked to connect the power sensor to the power meter reference output to calibrate the power sensor.

5.3 Measurement Procedure

The system that was built during this thesis can be understood as a test bench of an LSNA system. It is intended to implement and verify the calibration methods which have been introduced in chapter 3. Complete flexibility is provided to the user at various system settings at the cost of a more sophisticated initialization process that is depicted in figure 5.3 and described in what follows.
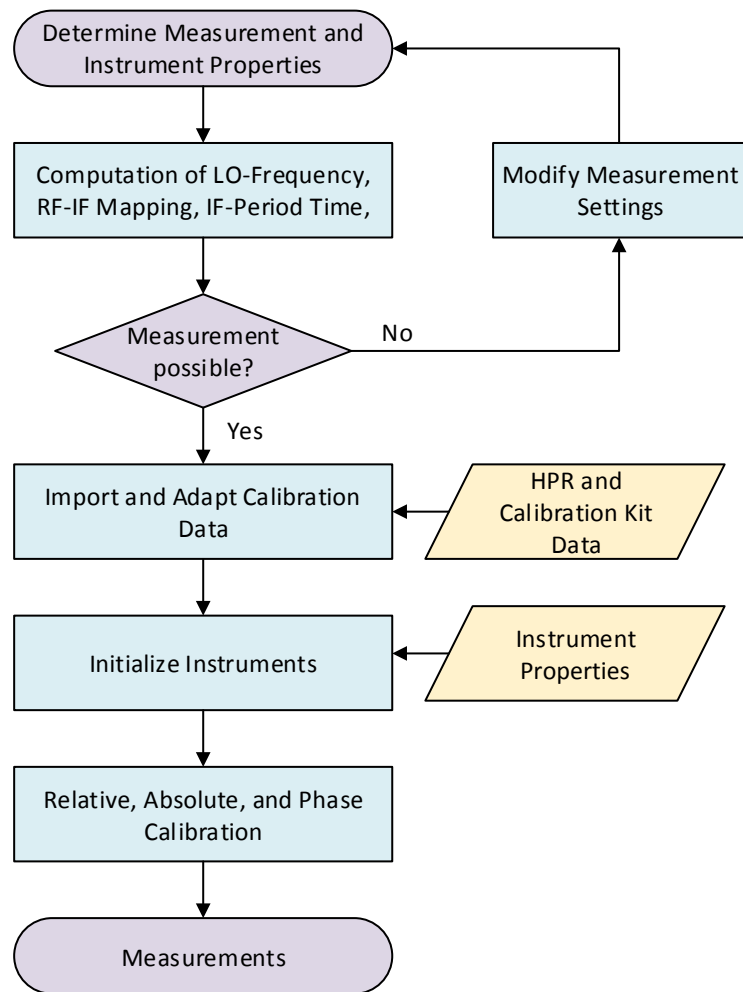
Figure 5.3: Procedure of system and instrument initialization, calibration, and measurement

Determine Measurement and Instrument Properties

Each measurement starts with the definition of some parameters, mainly all frequency components to be measured f_{meas} as well as the genders of the DUT ports. It should be kept in mind that the calibration has to be done for all these frequencies points. In the next step the HPR- and multitone-calibration frequencies must be determined. After that, a set of all possible LO frequencies $f_{LO,all}$ has to be declared to compute the most appropriate LO setting according to the guidelines in section 5.1. Based on the parameters above, the function "calc_lo_freq", which was implemented within this thesis, computes the LO frequency that leads to a maximum IF frequency tone spacing Δf_{IF} and a minimum IF period of time T_{IF}. This also corresponds to a small trigger period T_{trig}. Generally, it is not recommended to define all local oscillator frequencies (shown in table A.2) using this computation because this leads to long processing times and possibly very long IF periods which doesn't well match with the design guidelines or some system limits.

It turned out to be sufficient at the vast majority of cases to utilize the default settings which contain LO frequencies between $19\,\text{MHz}$ and $20\,\text{MHz}$ on a $50\,\text{Hz}$ grid. In combination with only integer multiples of $50\,\text{Hz}$ measurement frequencies, what will be fulfilled in almost all cases, it has the consequence that the default settings of the trigger generator ($T_{trig} = 1/50\,\text{Hz}$), and the oscilloscope ($T_{acquire} = 20\,\text{ms}$, $N_{ADC} = 500,000$) are always appropriate.

Propertiy	Symbol	Value
Measurement Freq.	f_{meas}	$2\,\text{MHz} - 12\,\text{GHz}$, $2\,\text{MHz}$ Spacing
Number of Tones	N_{Tones}	6,000
LO Freq.	f_{LO}	$19.2016\,\text{MHz}$
min. IF Tone Spacing	$\Delta f_{IF,min}$	$1.6\,\text{kHz}$
IF Period Time	T_{IF}	$0.625\,\text{ms}$
ADC Freq.	f_{ADC}	$25\,\text{MHz}$
Acquire Time	$T_{acquire}$	$20\,\text{ms}$
Recorded Samples	N_{ADC}	500,000
Trigger Freq.	$f_{trigger}$	$50\,\text{Hz}$

Table 5.2: Settings of a measurement example

Finally, the function "calc_lo_freq" will return a message whether the computing of a LO frequency was successful or not. In the first case the minimum IF tone spacing $\Delta f_{IF,min}$ and the IF signal period T_{IF} is returned, whereas if it was not possible, the computation must be started again using alternative parameters

for $f_{LO,all}$ and/or f_{meas}. An overview of an exemplary setup measurement is given in table 5.2.

Import Calibration Standards
The phase relationships and complex reflection coefficients of the Keysight U9391F harmonic phase reference, that is characterized up to $50\,\mathrm{GHz}$ in $10\,\mathrm{MHz}$ steps, is stored in a csv file. This data will be imported, and if necessary, interpolated to the HPR calibration frequencies. The data of the utilized male and female Rohde & Schwarz calibration kit ZV-Z132 are also deposited in a file. This data will be imported and used to calculate the complex transmission and reflection coefficients for all measurement frequencies. Currently, any other relative calibration standard can be imported by simply creating a new file. However, it is limited to elements that are defined by some electrical length and frequency dependent inductances (short) and capacitances (open), approximated by a third order polynomial.

Initialize Instruments
Generally, the connection establishment and the initialization of the instruments is accomplished utilizing methods described in section 5.2.2. The default settings of the downconverter and the oscilloscope have to be modified if necessary (cf. ADC settings in section 5.1). An exception is the reference generator which is not remote controlled in this LSNA prototype. Consequently, the trigger frequency must be manually selected according to the guidelines in section 5.1.

Calibration
Finally, all calibration measurements have to be done using the system configurations as depicted in figure 5.4. The only thing the user has to do is to connect the components (calibration standards) at each calibration step. All power and frequency settings, as well the recording will be made through the respective functions ("cal_solt", "cal_pwr", "cal_phase", "cal_mult"). After a complete calibration procedure, the error coefficients are fully defined and the actual measurement can be started.
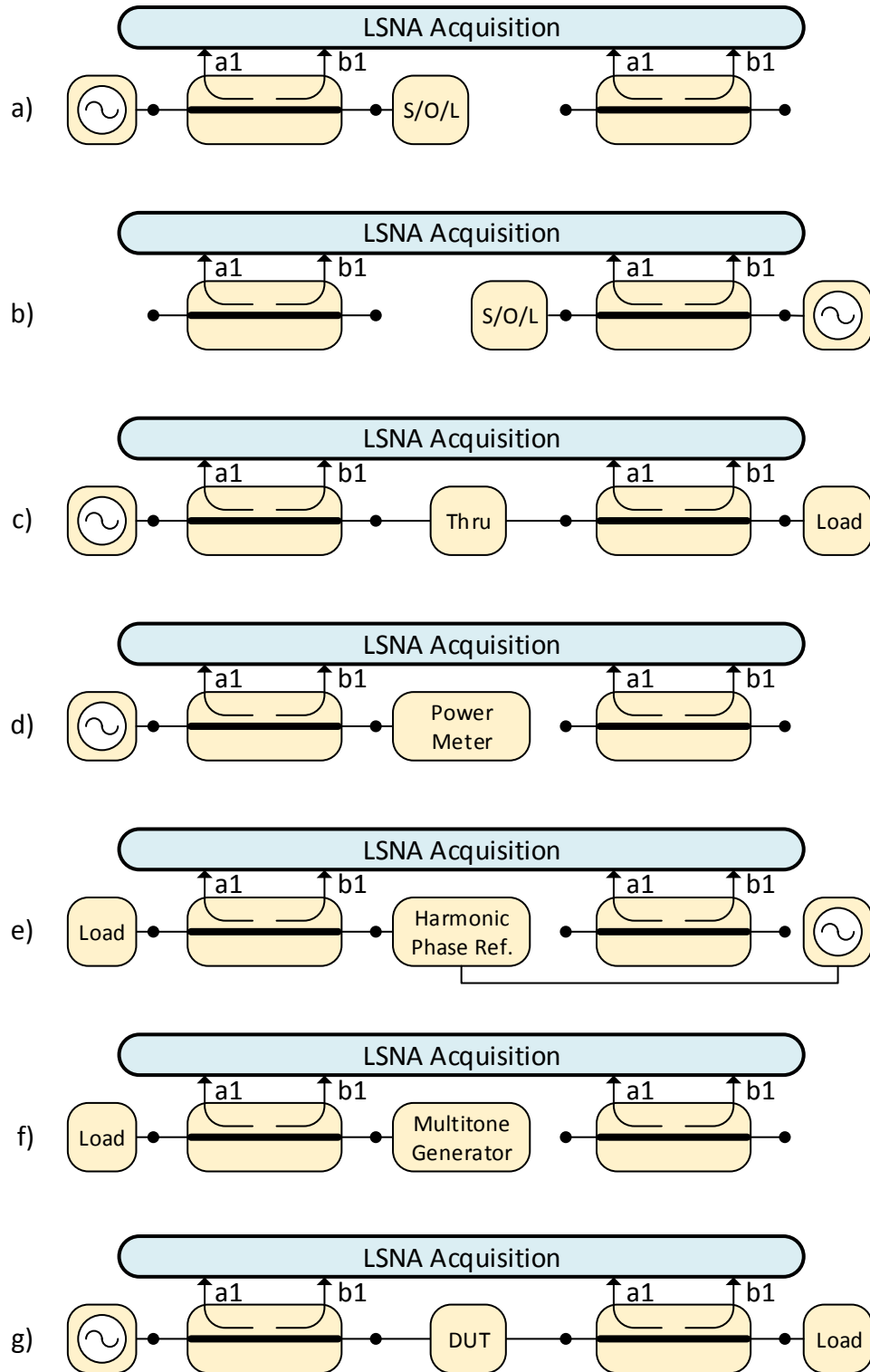
Figure 5.4: Hardware settings during a measurement initialization. a) relative calibration channel 1, b) relative calibration channel 2, c) relative thru calibration, d) absolute power calibration, e) HPR phase calibration, f) multitone phase calibration, g) DUT measurements

5.4 Verification of the Calibration Process

Various measurements have been made to verify the correct functionality of the system and the calibration. This mainly includes the questions, if the local oscillator and the trigger frequency is correctly computed to fulfil the design guidelines presented in section 5.1, and whether the calibration was correctly developed and implemented. After testing the correctness of the various frequency settings, some harmonic signals have been acquired to verify the operation of coherent sampling and to verify the correct descrambling operation of all measurement frequencies as described in section 2.1.3.
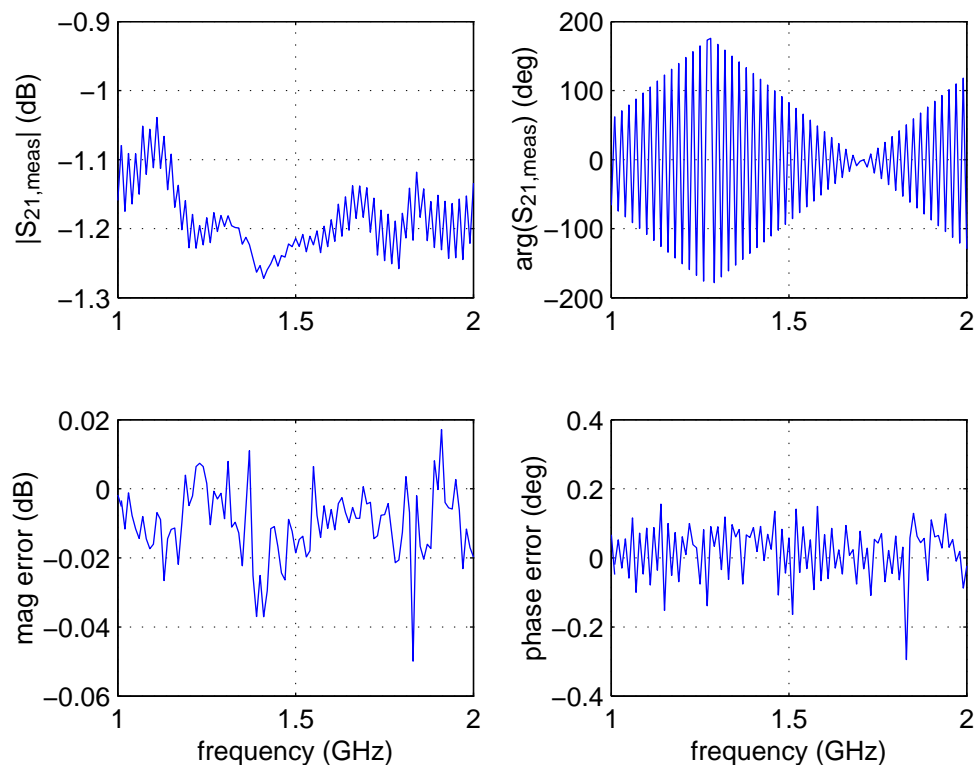
Figure 5.5: Relative calibration verification using the thru-calibration standard as DUT

The relative calibration can easily be verified utilizing the known calibration standards as DUTs. Figure 5.5 depicts the S_{21} parameter of a measurement of the thru-standard, that was also used at the calibration. The S_{21} parameter equals the ratio of the waves b_2 and a_1 at a specific frequency. At this measurement the frequencies are uniformly distributed in the range of $1\,\mathrm{GHz} - 2\,\mathrm{GHz}$ at a grid of $10\,\mathrm{MHz}$ while the LO frequency was adjusted to $19.701\,\mathrm{MHz}$.

The upper part of the figure shows the ratios of the raw measured values without error correction. It can be seen that especially the phase response at the right side is almost meaningless. The lower left part of figure 5.5 shows the magnitude error of the measured frequency response which is vanishingly small and contains only a measurement uncertainty of about 0.05 dB. It has to be noted, that the measurement is also equal to the amplitude response of the $|S_{21}^{DUT}|$ parameter because the thru-calibration element is considered as ideal and only specified by an electrical length during the calibration. The lower right part depicts the phase error between the angle of S_{21}^{DUT} and the specified phase response of the thru-element which shows a very small, and zero mean phase error. This and other S-parameter measurements demonstrate that the relative error coefficients have been determined correctly.
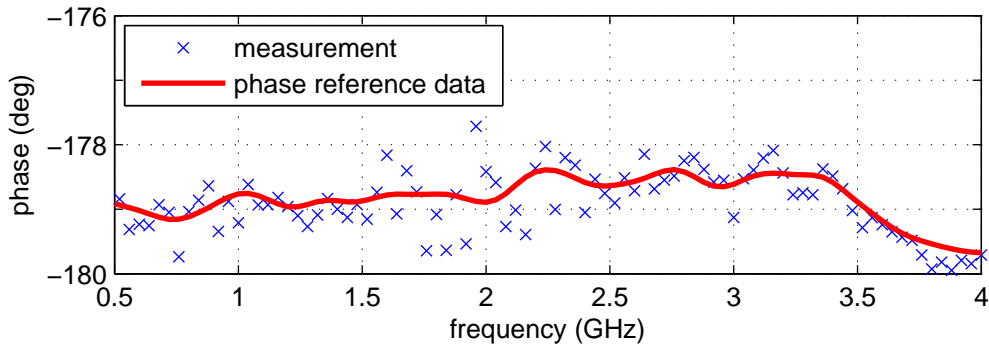
Figure 5.6: HPR Calibration Verification. $\arg\left(b_1^{DUT}\right)$, measured in the equal system configuration as at calibration.

Figure 5.6 shows the stored phase data of the harmonic phase reference in comparison to the phases of b_1^{DUT} measured, using the same system configuration as depicted in figure 5.4 e). A pulse repetition frequency of 40 MHz has been set for the HPR. The figure shows a small deviation of the measured angles in comparison to the stored angles with an RMS-error of 0.5°. Successive measurements show almost the same results. The phase relationships also remain almost constant after a new initialization of the phase reference up to a constant group delay. Due to this fact, it can be concluded that the HPR calibration procedure is correctly implemented.

The verification measurement that is depicted in figure 5.7 was calibrated using HPR harmonics at $\{...480, 520...\}$ MHz and 40 MHz wide multitone signals centered around the HPR frequencies. The LO frequency was adjusted to 19.9245 MHz. A multitone signal equal to the calibration multitone signal but slightly offset by 20 MHz was generated to verify the multitone calibration and the correct alignment between the multitone calibrations at adjacent HPR fre-

quencies. The upper part in figure 5.7 shows almost equal measured phases in comparison to the defined Shapiro Rudin phases (described in section 3.4.2).

A deeper investigation of the phase stability is depicted at the lower part of the figure which shows the phase errors between the calculated and measured signal phases. It must be noted, that the measurement error also contains an error of the generated signal which relates to the tolerances of the arbitrary waveform generator. Because of this additional error no further investigation and statement can be made about about the phase error.
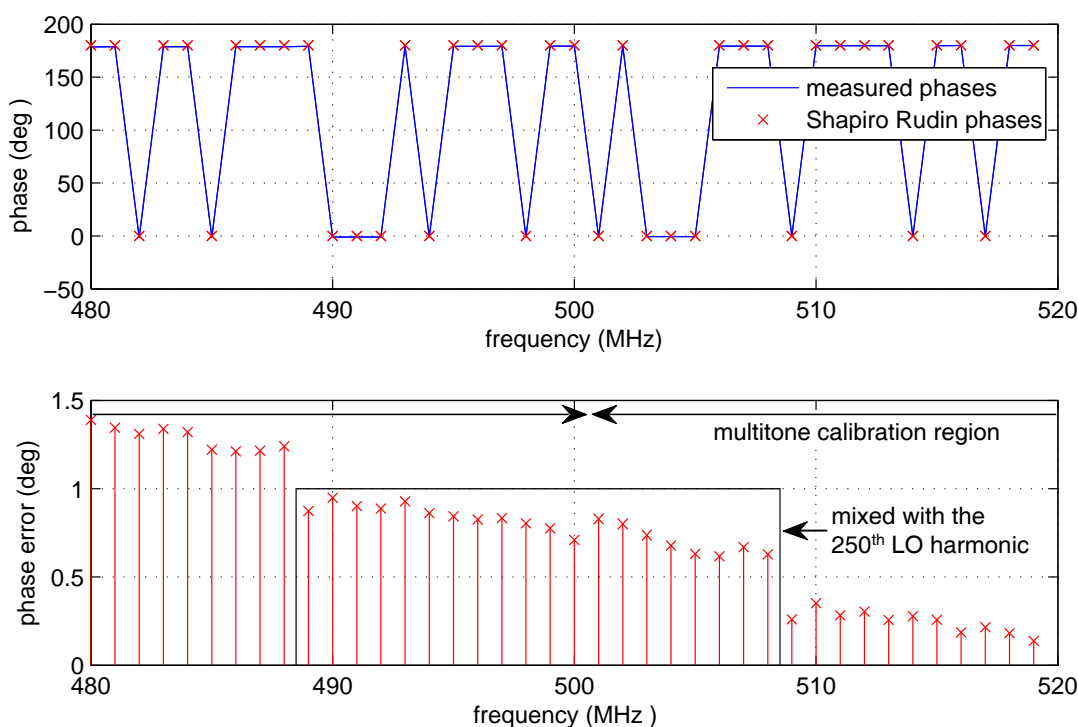
Figure 5.7: Multitone Calibration Verification. Measured phases of (b_1^{DUT} compared to the adjusted Shapiro Rudin phases

Nevertheless, it can be seen that there is only a small difference between the phases at 500 MHz and 501 MHz. Therefore, it can be argued that the HPR and the multitone calibration has been correctly developed and implemented. However, by comparing the phases between 488 MHz and 489 MHz as well as between 508 MHz and 509 MHz, a small step of about 0.3 degrees can be found. These frequencies correspond to limits at which the frequency tones are mixed with a different LO harmonic.

For example, in this measurement the tones between 489 MHz and 508 MHz are mixed with the 250th LO harmonic located at 498.11 MHz. Consequently,

this effect, which is also described in [14], originates from slightly different phases of the local oscillator at the calibration and the measurement and cannot be completely prevented because of some imperfections of the trigger generator.

5.5 Summary

In this chapter, the implementation and the verification of the custom large signal network analyzer framework that was built during this thesis has been described.

The evaluation of the local oscillator and the trigger frequency computed by the software has shown that no overlapping of the downconverted frequency components occurs in the IF bandwidth. Moreover, the IF tone spacing is maximized for a given set of measurement and LO frequencies. The presented verification measurements indicate that the measured data is coherently acquired for appropriately set frequency parameters as described in section 5.1). Furthermore, the system accomplishes correct IF to RF descrambling. Finally, relative and absolute measurements as discussed in section 5.4 demonstrated the correct implementation of the developed calibration techniques.

Chapter 6

Conclusion and Outlook

Within this thesis a custom large signal network analyzer was built to overcome some limitations of the existing commercial LSNA. The system was designed for fully calibrated measurements of arbitrary periodic signals using arbitrary frequency grids. Because the documentation of the downconverter Agilent N4464A has become public domain, it was possible to setup an LSNA based on this sampling downconverter as the "core" element.

Many characterization measurements have been conducted in order to determine the fundamental properties, possibilities, and limits of the system. All functionalities of the downconverter's individual parts have tested and verified. Moreover, input signals with different frequencies and input powers have been fed into the system to characterize the transfer characteristic of the RF and IF path as well as the linearity behavior of the downconverter. During this work some irregularities were detected and further investigated. For example, the time dependent phase noise phenomena of the step recovery diode which has resulted in limitations of the RF and IF frequency tone spacing.

The developed system consists of all essential components of an LSNA, as a source, a test set, a downconverter, and an acquisition module. In this thesis a four channel oscilloscope is utilized to acquire the IF signals. Due to the broadband capability, an additional trigger source is needed to obtain the same conditions in subsequent measurements. A Matlab LSNA software framework has been implemented, which assists the user in the stages of instrument initialization, calibration, and the measurement itself.

The calibration consists of a classical relative calibration, in which a SOLT calibration is implemented in this work, an absolute power calibration, and a phase calibration. In order to obtain calibrated broadband measurements, a combination of two phase calibration techniques, denoted as "HPR calibration" and

"multitone calibration", was developed and implemented. Finally, measurements have been performed to verify the different calibrations.

References

[1] W. V. Moer and L. Gomme, "Nvna versus lsna: enemies or friends?," *IEEE Microwave Magazine*, vol. 11, pp. 97–103, Feb 2010. 1, 4, 15, 34

[2] M. M. Corporation, *Large Signal Network Analyzer Technology - Preliminary Product Overview.* Application Note 5C-052, May 2003. 1, 2

[3] J. Verspecht, "Large-signal network analysis," *IEEE Microwave Magazine*, vol. 6, pp. 82–92, Dec 2005. 1, 2, 3, 13, 20

[4] A. Barel, "History of nonlinear microwave measurements." Vrije Universiteit Brussel. 1, 9

[5] "Large-signal network analysis. overview of the measurement capabilities of a large-signal network analyzer.," 2001. Agilent Technologies, Inc. 4

[6] J. Verspecht, F. Verbeyst, and M. vanden Bossche, "Network analysis beyond s-parameters: Characterizing and modeling component behaviour under modulated large-signal operating conditions," in *ARFTG Conference Digest-Fall, 56th*, vol. 38, pp. 1–4, Nov 2000. 4

[7] G. Magerl, "Advanced rf techniques," 2013. University Lecture. 8

[8] J. Verspecht, *Calibration of a Measurement System for High Frequency Nonlinear Devices.* Dissertation, Vrije Universiteit Brussel, Nov 2001. 9, 14

[9] M. Myslinski, G. Pailloncy, G. Avolio, F. Verbeyst, M. V. Bossche, and D. Schreurs, "State-of-the-art microwave device characterization using large-signal network analyzers," in *Mixed Design of Integrated Circuits and Systems (MIXDES), 2010 Proceedings of the 17th International Conference*, pp. 91–95, June 2010. 13

[10] P. Roblin, *Nonlinear RF Circuits and Nonlinear Vector Network Analyzers.* July 2011. 13, 18, 20, 44

[11] H. Packard, *Fundamentals of RF and Microwave Power Measurements.* Application Note 64-1A, June 1998. 18, 19

[12] T. V. den Broeck and J. Verspecht, "Calibrated vectorial nonlinear-network analyzers," in *Microwave Symposium Digest, 1994., IEEE MTT-S International*, pp. 1069–1072 vol.2, May 1994. 19

[13] S. Boyd, "Multitone signals with low crest factor," *IEEE Transactions on Circuits and Systems*, vol. 33, pp. 1018–1022, Oct 1986. 23

[14] Y. Ko, P. Roblin, S. Myoung, J. Strahler, F. D. Groote, and J. P. Teyssier, "Multi-harmonic broadband measurements using an large signal network analyzer," in *Microwave Measurements Conference (ARFTG), 2010 75th ARFTG*, pp. 1–6, May 2010. 24, 44, 56

[15] K. A. Remley, D. F. Williams, D. Schreurs, and M. Myslinski, "Measurement bandwidth extension using multisine signals: Propagation of error," *IEEE Transactions on Microwave Theory and Techniques*, vol. 58, pp. 458–467, Feb 2010. 24

[16] M. E. Yaagoubi, G. Neveuxm, D. Barataud, J. Nebus, and J. Verspecht, "Accurate phase measurements of broadband multitone signals using a specific configuration of a large signal network analyzer," in *Microwave Symposium Digest, 2006. IEEE MTT-S International*, pp. 1448–1451, June 2006. 24

[17] S. Vandenplas, J. Verspecht, F. Verbeyst, E. Vandamme, and M. V. Bossche, "Calibration issues for the large signal network analyzer (lsna)," in *ARFTG Conference Digest, Fall 2002. 60th*, pp. 99–106, Dec 2002. 25, 28

[18] M. M. Corporation, *Large Signal Network Analyzer - System Manual.* MT4463-38, 2004. 30, 32, 35, 38, 63

[19] J.-P. Teyssier, "Scpi vocabulary for an embedded controller of the lsna and test set system." XLIM France, Nov 2013. 37

[20] R. Hogan, "Sampling signal analyzer - analog signal processing overview." Hewlett Packard, April 1988. 37

[21] "Wave expert 100h - operators manual." LeCroy, July 2007. 39

[22] M. M. Corporation, *Large Signal Network Analyzer - Programmers Manual.* MT4463-37, 2004. 42

[23] I. Corporation, *A Theoretical View of Coherent Sampling.* Application Note 9705, June 1997. 43

[24] "libusb library documentation." `http://www.libusb.org/`. Accessed Mach 30, 2016. 47

[25] T. L. Robinson, "libusbk 3.0 library documentation." `http://libusbk.sourceforge.net/UsbK3/index.html`. Accessed Mach 30, 2016. 47

[26] "Agilent infiniivision 6000 series oscilloscopes - programmers reference." Agilent Technologies, April 2008. 48

Appendices

N4464A Specifications

Based on the LSNA system manual [18] and all characterization measurements, the existing specifications have been verified and modified to the following overview:

A.1   Connector Descriptions

Connector label	Type	Usage
"a1"	2.4 mm female input	RF input, corresponding to the incident wave at port 1
"b1"	2.4 mm female input	RF input, corresponding to the reflected wave at port 1
"a2"	2.4 mm female input	RF input, corresponding to the incident wave at port 2
"b2"	2.4 mm female input	RF input, corresponding to the reflected wave at port 2

Table A.1: Front panel connector description of the MT4464 Sampling Converter.

Connector label	Type	Usage
"(a1) CHANNEL 1"	BNC output	IF output, corresponding "a1" RF input
"(b1) CHANNEL 2"	BNC output	IF output, corresponding "a1" RF input
"(a2) CHANNEL 3"	BNC output	IF output, corresponding "a1" RF input
"(b2) CHANNEL 4"	BNC output	IF output, corresponding "a1" RF input
"10 MHz REF"	BNC input	Input for the external 10 MHz reference clock
"GB-IB"	GPIB input/output	Allows the PC to control the internal hardware of the downconverter. The default GPIB address is 10.
"DC IN"	DB-25 female	DC power supply

Table A.2: Rear panel connector description of the MT4464 Sampling Converter.

A.2   Specifications

Measurement Specifications

Property	Value
RF frequency range	$DC - 50\,GHz$
IF frequency range	$DC - 10\,MHz$
Minimum distance of RF/IF tones (limited by the phase noise of the SRD)	$1\,kHz$
Maximum number of of RF tones (in case of equally IF distribution)	10,000

Table A.3: Frequency specifications

Property	Value
Damage level (at $0\,\mathrm{dB}$ input attenuation)	$10\,\mathrm{dBm}$ (peak $\pm 1\,\mathrm{V}$ DC $+$ AC)
Harmonic mixer operating range	$< 0\,\mathrm{dBm}$
Step attenuator operating range	$+27\,\mathrm{dBm}$
Step attenuation (input att.)	$60\,\mathrm{dB}$, $10\,\mathrm{dB}$ steps
Step gain (output gain)	$36\,\mathrm{dB}$, $6\,\mathrm{dB}$ steps
Input Impedance	$50\,\Omega$
Input Coupling	DC / AC / GND

Table A.4: Power specifications

Linear Operating Range

The following table shows the maximum input power that the output amplifier gets not into compression and a spurious free dynamic range $> 70\,\mathrm{dB}$ is obtained for different gain settings and $0\,\mathrm{dB}$ input attenuation.

Gain Setting g_{amp} (dB)	0	6	12	18	24	30	36
Input Power P_{in} (dB)	–6	–6	–6	–6	–6	–12	–18

Table A.5: Power specifications

Fractional-N Specifications

Property	Value
Frequency span	$10 - 25\,\mathrm{MHz}$
Frequency resolution	$1\,\mathrm{Hz}$
Reference clock input	$10\,\mathrm{MHz}$

Table A.6: fractional-N Specifications

U9391-F Harmonic Phase Reference Commands

Initialization Example
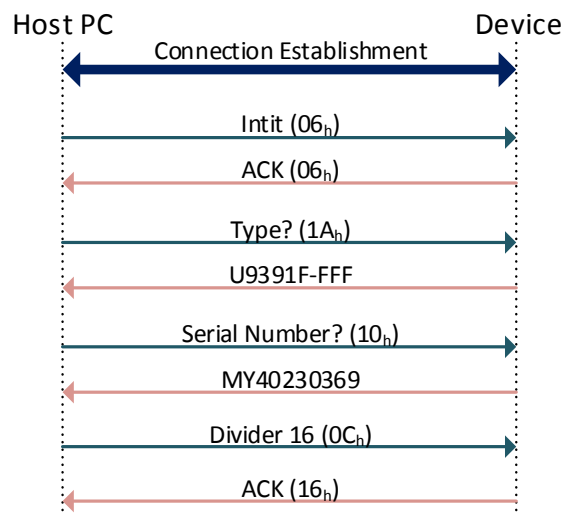
Figure B.1: Example of a Initialization of the phase reference "Keysight U9391-F"

Commands

The following gives an overview of all known commands of the Agilent U9391F HPR. Down means transfer from the host to the device. It is not recommended to test other commands as listed because of the risk to deleting data.

Down (hex)	Up (hex)	Up (ASCII)	Meaning
06	06		initialization
08	08		divider 1
09	09		divider 2
0A	0A		divider 4
0B	0B		divider 8
0C	0C		divider 16
0D			delete time
0E		`07:25...........` `...............`	time?
0F			delete serial number

10		`MY40230369......`
		 `...............`
		 `...............`
		 `...............`
			ask for serial number?

11	0f		unknown
12 00 XX XX XX			ask for calibration data? returns a block of 64 bytes containing the calibration data
13			no answer
14	B8 88 00 00		unknown
15			no answer
16			no answer
17			no answer
18		`260914..........` `...............`	ask for date?

1A		`U9391F-FFF......`
		 `...............`
		 `...............`
		 `...............`
			ask for type?

1B			no answer
1C		`A1..............` `...............`	unknown

Table B.1: U9391F commands